AWARD NUMBER: W81XWH-17-1-0251

TITLE: The role of PARP2 in prostate cancer

PRINCIPAL INVESTIGATOR: Li Jia, Ph.D.

CONTRACTING ORGANIZATION: Brigham and Women's Hospital

REPORT DATE: July 2019

TYPE OF REPORT: Annual

PREPARED FOR: U.S. Army Medical Research and Materiel Command
Fort Detrick, Maryland 21702-5012

DISTRIBUTION STATEMENT: Approved for Public Release;
Distribution Unlimited

REPORT DOCUMENTATION PAGE

Form Approved
OMB No. 0704-0188

1. REPORT DATE	2. REPORT TYPE	3. DATES COVERED
July 2019	Annual	July 1, 2018—June 30, 2019

4. TITLE AND SUBTITLE

The role of PARP2 in prostate cancer

5a. CONTRACT NUMBER

5b. GRANT NUMBER
W81XWH-17-1-0251

5c. PROGRAM ELEMENT NUMBER

6. AUTHOR(S)

Li Jia

E-Mail: ljia@bwh.harvard.edu

5d. PROJECT NUMBER

5e. TASK NUMBER

5f. WORK UNIT NUMBER

7. PERFORMING ORGANIZATION NAME(S) AND ADDRESS(ES)

Brigham and Women's Hospital
75 Francis Street
Boston, MA 02115-6110

8. PERFORMING ORGANIZATION REPORT NUMBER

9. SPONSORING / MONITORING AGENCY NAME(S) AND ADDRESS(ES)

U.S. Army Medical Research and Materiel Command
Fort Detrick, Maryland 21702-5012

10. SPONSOR/MONITOR'S ACRONYM(S)

11. SPONSOR/MONITOR'S REPORT NUMBER(S)

12. DISTRIBUTION / AVAILABILITY STATEMENT

Approved for Public Release; Distribution Unlimited

13. SUPPLEMENTARY NOTES

14. ABSTRACT

Androgen receptor (AR) is a key driver of prostate cancer (PCa) growth and progression. Understanding the factors influencing AR-mediated gene expression provides new opportunities for therapeutic intervention. Poly(ADP-ribose) Polymerase (PARP) is a family of enzymes, which post-translationally modify a range of proteins and regulate many different cellular processes. PARP1 and PARP2 are two well-characterized PARP members, whose catalytic activity is induced by DNA-strand breaks and responsible for multiple DNA damage repair pathways. PARP inhibitors are promising therapeutic agents that show synthetic lethality against many types of cancer with homologous recombination DNA-repair deficiency. Here, we show that beyond DNA damage repair function, PARP2, but not PARP1, is a critical component in AR transcriptional machinery through interacting with the pioneer factor FOXA1 and facilitating AR recruitment to genome-wide prostate-specific enhancer regions. Analyses of PARP2 expression at both mRNA and protein levels show significantly higher expression of PARP2 in primary PCa tumors than in benign prostate tissues, and even more so in castration-resistant prostate cancer tumors. Selective targeting of PARP2 by genetic or pharmacological means blocks interaction between PARP2 and FOXA1, which in turn attenuates AR-mediated gene expression and inhibits PCa growth. Next-generation anti-androgens act through inhibiting androgen synthesis or blocking ligand binding. Selective targeting of PARP2, however, may provide an alternative therapeutic approach for AR inhibition by disruption of FOXA1 function, which may be beneficial to patients, irrespective of their DNA-repair deficiency status.

15. SUBJECT TERMS
Prostate cancer, androgen receptor, PARP2, PARP inhibitor

16. SECURITY CLASSIFICATION OF:			17. LIMITATION OF ABSTRACT	18. NUMBER OF PAGES	19a. NAME OF RESPONSIBLE PERSON
a. REPORT	b. ABSTRACT	c. THIS PAGE			USAMRMC
Unclassified	Unclassified	Unclassified	Unclassified	41	19b. TELEPHONE NUMBER *(include area code)*

Table of Contents

Page

1. INTRODUCTION:

Androgen receptor (AR)-mediated gene expression plays a key role in prostate cancer (PCa) growth and progression. Androgen deprivation therapy (ADT) is an effective treatment for advanced PCa. However, patients who initially respond to the therapy inevitably develop incurable castration-resistant prostate cancer (CRPC). The next-generation anti-androgens have shown benefits for CRPC patients; the increased length of survival, however, is measured in months. While AR-independent mechanisms have been identified, the growth of therapy-resistant tumor is still largely AR-dependent due to AR amplification, point mutations, splice variants, and ligand-independent AR activation. Notably, AR cistrome and transcriptional activity have been studied in great detail to be prominently dictated by the pioneer factor FOXA1. Interestingly, genome sequencing studies have revealed that FOXA1 is one of the most frequently mutated genes in primary PCa and even more common in metastatic CRPC. Aberrant FOXA1 function is implicated in PCa development and progression, likely through its impact on AR cistrome. Therefore, inhibition of AR through targeting FOXA1 is an attractive therapeutic approach for CRPC.

Poly(ADP-ribose) polymerase (PARP) is a family of enzymes that uses NAD+ as a substrate to synthesize and transfer ADP-ribose polymers onto target proteins. This post-translational modification is known as poly(ADP-ribosyl)ation (PARylation), which is involved in various cellular processes, including DNA damage repair, modulation of chromatin structure, transcription regulation, and cell division. PARP inhibitors (PARPi) are a new type of targeted therapy, which works based on a concept of synthetic lethality. The US FDA has approved four PARPi (olaparib, niraparib, talazoparib, and rucaparib) for the treatment of advanced ovarian cancer and breast cancer patients with BRCA mutations. Recent clinical trials have also shown promising results of olaparib in the treatment of metastatic CRPC patients who have homologous recombination (HR) DNA-repair deficiency. It should be noted that current clinically-used PARPi target both PARP1 and PARP2. While studies have linked both PARP1 and PARP2 with PCa development and progression, the distinct roles of PARP1 vs. PARP2 remain unclear. In this project, we have discovered a functional connection between PARP2, AR, and FOXA1 in PCa cells. We demonstrate that PARP2 is a key component in AR-mediated transcription through interacting with the pioneer factor FOXA1 and is required for PCa growth. The objective of this project is to further determine the oncogenic role of PARP2 in PCa growth and progression, and establish the basis for therapeutic targeting of PARP2 in PCa. We will determine whether selective targeting of PARP2 inhibits PCa growth and progression in specific pre-clinical settings, and elucidate the AR-dependent mechanisms by which PARP2 promotes PCa growth and metastasis. The successful implementation of this project will not only greatly advance our mechanistic understanding of development of aggressive PCa, but also have important implications for development of therapeutic strategies by targeting PARP2 alone or in combination with either AR antagonists or DNA damage agents.

2. KEYWORDS:

prostate cancer, androgen receptor, PARP2, PARP inhibitor, DNA repair

3. ACCOMPLISHMENTS:

What were the major goals of the project?

The major goal of this project is to determine the oncogenic role of PARP2 in PCa growth and progression, and establish the basis for therapeutic targeting of PARP2 in PCa. We have proposed two specific aims. In aim 1, we will determine whether selective targeting PARP2 inhibits

PCa growth and progression in specific pre-clinical settings. In aim 2, we will determine the AR-dependent mechanisms by which PARP2 promotes PCa growth and metastasis.

The approved SOW is described in the next section.

What was accomplished under these goals?

Here, we breakdown our accomplishments by each of the tasks in the SOW:

Aim 1: Determine whether selective targeting PARP2 inhibits PCa growth and progression in specific pre-clinical settings.

Major Task 1

Subtask 1: In vitro cell growth studies (Months 1-6)

We have completed this subtask in year 1. We have shown that knockdown or knockout of PARP2 significantly inhibits AR-positive PCa cell growth using multiple assays in a number of PCa cell lines, demonstrating that PARP2 is required for PCa growth in vitro.

Subtask 2: In vitro cell migration/invasion studies (Months 1-6)

We have completed this subtask in year 1. We have found that knockdown or knockout of PARP2 has a minor effect on PCa cell migration/invasion in vitro, indicating the PARP2 protein has more important roles in PCa cell proliferation compared to migration or potential metastasis.

Subtask 3: Determine whether BRCA1/2 status affects cell response to PARP inhibition (Months 1-6)

We have completed this subtask in year 1. We have found that loss of BRCA1/2 makes PCa cells more sensitive to pan-PARP inhibitors (such as olaparib), but it does not affect selective PARP2 inhibitor UPF-1069, supporting the notion that patients may benefit from selective PARP2 inhibition regardless of their DNA-repair deficiency status.

Major Task 2

Subtask 1: PARP1/2 knockout xenograft models (Months 7-18)

We have completed this subtask in years 1-2. We implanted the PARP1 and PARP2 knockout LNCaP cell lines subcutaneously into immunodeficient mice, and found that depletion of either PARP1 or PARP2 gene completely diminished tumorigenic potential of LNCaP cells.

Subtask 2: Xenograft models with drug treatment (anti-androgen + PARP inhibitors) (Months 13-24)

We have postponed this subtask and will complete it in year 3.

Subtask 3: Xenograft models with drug treatment (combination of PARP inhibitors) (Months 19-30)

We will complete this subtask in year 3.

Milestone(s) Achieved:

We have published our work in PNAS in July 2019.

Selective targeting of PARP-2 inhibits androgen receptor signaling and prostate cancer growth through disruption of FOXA1 function. Gui B, Gui F, Takai T, Feng C, Bai X, Fazli L, Dong X, Liu S, Zhang X, Zhang W, Kibel AS, Jia L. Proc Natl Acad Sci U S A. 2019 Jul 16;116(29):14573-14582. PMID:31266892

Specific Aim 2: Determine the AR-dependent mechanism by which PARP2 promotes PCa growth and metastasis

Major Task 3

Subtask 1: Determine whether and how PARP2 affects AR-mediated transcription (Months 19-30)

We have completed this subtask ahead of schedule in year 2. We have discovered that PARP2 impacts AR and FOXA1 binding genome-wide using ChIP-seq and RNA-seq analyses.

Subtask 2: Define genomic sites targeted by PARP inhibitors (Months 25-36)

This subtask will be completed in year 3.

Subtask 3: Determine interaction between PARP2 and FOXA1 (Months 31-36)

We have completed this subtask ahead of schedule in year 2. We have shown that PARP2 directly interacts with FOXA1 using co-IP and GST pull-down assays. We have further demonstrated that PARP2 enzymatic activity is not required for its role in AR/FOXA1-mediated transcriptional regulation.

All results up to date have now published in PNAS. The paper is attached in **Appendices**.

What opportunities for training and professional development has the project provided?

Dr. Bin Gui, who is the first author in the PNAS paper, has completed his postdoctoral training in the PI's lab. He has now joined Ribon Therapeutics in Cambridge Massachusetts as a senior scientist working on the development of novel PARP inhibitors.

How were the results disseminated to communities of interest?

Nothing to Report.

What do you plan to do during the next reporting period to accomplish the goals?

In year 3, we will complete the xenograft studies in Major Task 2 (subtask 2 & 3) and define genomic sites targeted by PARP inhibitors in Major Task 3 (subtask 2).

4. IMPACT:

What was the impact on the development of the principal discipline(s) of the project?

While androgen deprivation therapy (ADT) has been the mainstay of treatment for advanced PCa leading to initial response and durable remission, incurable CRPC invariably develops. Importantly, AR activity remains critical for CRPC tumor growth. Despite the significant research advances in PCa biology and development of next-generation anti-androgens, there has been limited progress in the management of CRPC when direct AR-targeted therapies fail. PARP2, which enhances AR-mediated transcription through interaction with the pioneer factor FOXA, is a druggable target. Targeting PARP2 may potentially provide an alternative therapeutic approach for AR inhibition without involving AR ligand binding. Our discoveries will not only greatly advance

our mechanistic understanding of development of aggressive PCa, but also have important implications for development of therapeutic strategies by targeting PARP2 alone or in combination with either AR antagonists or DNA damage agents.

What was the impact on other disciplines?

Nothing to Repot.

What was the impact on technology transfer?

Nothing to Report.

What was the impact on society beyond science and technology?

Nothing to Report.

5. CHANGES/PROBLEMS:

We have rearranged the order of our tasks. In year 2, we have completed the subtasks 1 & 3 in Major Task 3, which was originally planned for year 3. On the other hand, we have postponed the subtask 2 in Major Task 2 until year 3. These tasks are listed as follows:

Major Task 2:

Subtask 2: Xenograft models with drug treatment (anti-androgen + PARP inhibitors) (Months 13-24) – postponed.

Major Task 3:

Subtask 1: Determine whether and how PARP2 affects AR-mediated transcription (Months 19-30) – completed ahead of schedule.

Subtask 3: Determine interaction between PARP2 and FOXA1 (Months 31-36) – completed ahead of schedule.

The reason for this change is: During the PNAS peer review process, the reviewers requested mechanistic details regarding PARP2/FOXA1 interaction. We then made efforts to address these questions first. We now have included substantial new results in our publication.

6. PRODUCTS:

Publications

Selective targeting of PARP2 inhibits androgen receptor signaling and prostate cancer growth through disruption of FOXA1 function. Gui B, Gui F, Takai T, Feng C, Bai X, Fazli L, Dong X, Liu S, Zhang X, Zhang W, Kibel AS, Jia L. **Proc Natl Acad Sci U S A.** 2019 Jul 16;116(29):14573-14582. PMID:31266892

The paper is attached in **Appendices**.

Presentations

Dr. Li Jia (PI) gives a poster presentation at the "Hormone-Dependent Cancers" Gordon Research Conference, August 4-9, 2019, Newry, ME.

The title is "Selective Targeting of PARP-2 Inhibits Androgen Receptor Signaling and Prostate Cancer Growth Through Disruption of FOXA1 Function"

Other Products

We have generated several PARP1 and PARP2 knockout prostate cancer cell lines.

7. PARTICIPANTS & OTHER COLLABORATING ORGANIZATIONS:

What individuals have worked on the project?

Name:	*Li Jia*
Project Role:	*PI*
Researcher Identifier (e.g. ORCID ID):	*https://orcid.org/0000-0003-4017-1157*
Nearest person month worked:	*2.4 months*
Contribution to Project:	*Dr. Jia directs all aspects of the proposed research on a daily basis.*
Funding Support:	*No other funding support.*

Name:	*Bin Gui*
Project Role:	*Postdoctoral fellow*
Researcher Identifier (e.g. ORCID ID):	*https://orcid.org/0000-0001-6168-7262*
Nearest person month worked:	*2 months*
Contribution to Project:	*Dr. Gui has performed work on all aspects of the proposed molecular biology and xenograft mouse models.*
Funding Support:	*No other funding support.*

Name:	*Fu Gui*
Project Role:	*Postdoctoral fellow*
Researcher Identifier (e.g. ORCID ID):	
Nearest person month worked:	*8 months*

Contribution to Project:	*Dr. Gui has performed work on some of the proposed molecular biology work.*
Funding Support:	*No other funding support.*

Name:	*Tomoaki Takai*
Project Role:	*Postdoctoral fellow*
Researcher Identifier (e.g. ORCID ID):	
Nearest person month worked:	*2 months*
Contribution to Project:	*Dr. Takai has performed work on some of the proposed molecular biology work.*
Funding Support:	*No other funding support.*

Has there been a change in the active other support of the PD/PI(s) or senior/key personnel since the last reporting period?

Nothing to Report.

What other organizations were involved as partners?

Nothing to Report.

8. SPECIAL REPORTING REQUIREMENTS

Not Applicable.

9. APPEDICES:

The PNAS paper is attached.

Selective targeting of PARP-2 inhibits androgen receptor signaling and prostate cancer growth through disruption of FOXA1 function

Bin Gui[a], Fu Gui[a], Tomoaki Takai[a], Chao Feng[a], Xiao Bai[a], Ladan Fazli[b], Xuesen Dong[b], Shuai Liu[c], Xiaofeng Zhang[c], Wei Zhang[c], Adam S. Kibel[a,1], and Li Jia[a,1]

[a]Division of Urology, Department of Surgery, Brigham and Women's Hospital, Harvard Medical School, Boston, MA 02115; [b]Department of Urologic Sciences, Vancouver Prostate Centre, University of British Columbia, Vancouver, BC V6H 3Z6, Canada; and [c]Department of Chemistry, University of Massachusetts Boston, Boston, MA 02125

Edited by Bert W. O'Malley, Baylor College of Medicine, Houston, TX, and approved June 11, 2019 (received for review May 23, 2019)

Androgen receptor (AR) is a ligand-activated transcription factor and a key driver of prostate cancer (PCa) growth and progression. Understanding the factors influencing AR-mediated gene expression provides new opportunities for therapeutic intervention. Poly(ADP-ribose) Polymerase (PARP) is a family of enzymes, which posttranslationally modify a range of proteins and regulate many different cellular processes. PARP-1 and PARP-2 are two well-characterized PARP members, whose catalytic activity is induced by DNA-strand breaks and responsible for multiple DNA damage repair pathways. PARP inhibitors are promising therapeutic agents that show synthetic lethality against many types of cancer (including PCa) with homologous recombination (HR) DNA-repair deficiency. Here, we show that, beyond DNA damage repair function, PARP-2, but not PARP-1, is a critical component in AR transcriptional machinery through interacting with the pioneer factor FOXA1 and facilitating AR recruitment to genome-wide prostate-specific enhancer regions. Analyses of PARP-2 expression at both mRNA and protein levels show significantly higher expression of PARP-2 in primary PCa tumors than in benign prostate tissues, and even more so in castration-resistant prostate cancer (CRPC) tumors. Selective targeting of PARP-2 by genetic or pharmacological means blocks interaction between PARP-2 and FOXA1, which in turn attenuates AR-mediated gene expression and inhibits AR-positive PCa growth. Next-generation antiandrogens act through inhibiting androgen synthesis (abiraterone) or blocking ligand binding (enzalutamide). Selective targeting of PARP-2, however, may provide an alternative therapeutic approach for AR inhibition by disruption of FOXA1 function, which may be beneficial to patients, irrespective of their DNA-repair deficiency status.

PARP-2 | PARP inhibitor | androgen receptor | FOXA1 | prostate cancer

Androgen receptor (AR)-mediated gene expression plays a key role in prostate cancer (PCa) growth and progression. Androgen deprivation therapy (ADT) is an effective treatment for advanced PCa. However, patients who initially respond to the therapy inevitably develop incurable castration-resistant prostate cancer (CRPC). The next-generation antiandrogens have shown benefits for CRPC patients; the increased length of survival, however, is measured in months (1, 2). While AR-independent mechanisms have been identified (such as glucocorticoid receptor activation and neuroendocrine transdifferentiation), the growth of therapy-resistant tumor is still largely AR-dependent due to AR amplification, point mutations, splice variants, and ligand-independent AR activation (3). Notably, AR cistrome and transcriptional activity have been studied in great detail to be prominently dictated by the pioneer factor FOXA1 (4). FOXA1 binds the enhancer regions in the genome, increases local chromatin accessibility, and facilitates the recruitment of AR (5, 6). Interestingly, genome sequencing studies have revealed that FOXA1 is one of the most frequently mutated genes in primary PCa and even more common in metastatic CRPC (7, 8). Aberrant FOXA1 function is implicated in PCa development and progression, likely through its impact on AR cistrome. Therefore, inhibition of AR through targeting FOXA1 is an attractive therapeutic approach for CRPC.

Poly(ADP-ribose) polymerase (PARP) is a family of enzymes that uses NAD^+ as a substrate to synthesize and transfer ADP-ribose polymers onto target proteins. This posttranslational modification is known as poly(ADP-ribosyl)ation (PARylation), which is involved in various cellular processes, including DNA damage repair, modulation of chromatin structure, transcription regulation, and cell division (9). PARP inhibitors (PARPis) are a new type of targeted therapy, which works based on a concept of synthetic lethality. Cancer cells lacking BRCA1 or BRCA2 depend instead on PARP-regulated DNA repair and are hypersensitive to PARP inhibition (10, 11). The US Food and Drug Administration (FDA) has approved four PARPis (olaparib, niraparib, talazoparib, and rucaparib) for the treatment of advanced ovarian cancer and breast cancer patients with BRCA mutations. Recent clinical trials have also shown promising results of olaparib in the treatment of metastatic CRPC patients who have homologous recombination (HR) DNA-repair deficiency (12, 13). It should be noted that current clinically used PARPis target both PARP-1 and PARP-2. The mechanisms of action of PARPis with regard to their effects in cancer cells is largely based on PARP-1

Significance

While androgen deprivation therapy (ADT) has been the mainstay of treatment for advanced prostate cancer (PCa) leading to initial response and durable remission, incurable castration-resistant prostate cancer (CRPC) invariably develops. Importantly, androgen receptor (AR) activity remains critical for CRPC tumor growth. Despite the significant research advances in PCa biology and development of next-generation antiandrogens, there has been limited progress in the management of CRPC when direct AR-targeted therapies fail. PARP-2, which enhances AR-mediated transcription through interaction with the pioneer factor FOXA, is a druggable target. Targeting PARP-2 may potentially provide an alternative therapeutic approach for AR inhibition without involving AR ligand binding.

Author contributions: A.S.K. and L.J. designed research; B.G., F.G., T.T., C.F., X.B., L.F., X.D., S.L., X.Z., W.Z., and L.J. performed research; B.G., L.F., X.D., W.Z., A.S.K., and L.J. analyzed data; and B.G. and L.J. wrote the paper.

The authors declare no conflict of interest.

This article is a PNAS Direct Submission.

Data deposition: All ChIP-seq and RNA-seq data have been deposited in the Gene Expression Omnibus (GEO) database, https://www.ncbi.nlm.nih.gov/geo (accession no. GSE114275).

[1]To whom correspondence may be addressed. Email: akibel@bwh.harvard.edu or ljia@bwh.harvard.edu.

This article contains supporting information online at www.pnas.org/lookup/suppl/doi:10.1073/pnas.1908547116/-/DCSupplemental.

Published online July 2, 2019.

function. PARP-2 is the closest paralog of PARP-1. Biochemical and genetic studies have provided strong evidence of key shared functions of PARP-1 and PARP-2 in response to DNA-strand breaks although PARP-2 contributes only 10% of total cellular PARP enzymatic activity (14, 15). Despite functional redundancy, studies have shown that PARP-2 has unique biological functions distinct from PARP-1. Genetic disruption of PARP-2, but not of PARP-1, affects specific differentiation processes, including adipogenesis, the survival of thymocytes, and spermatogenesis (16–18). In addition, PARP-2 is associated with different protein complexes and implicated in the maintenance of heterochromatin integrity of centromeres, telomeres, and X chromosome inactivation (19–21). It has been increasingly shown that PARP-2 is involved in transcriptional regulation. PARP-2 acts as a cofactor for several transcription factors, including nuclear receptors such as peroxisome proliferator-activated receptors (PPARs) and estrogen receptor (ER) α (16, 22, 23). Thus, it is conceivable that the clinical application of PARPi for cancer treatment will require further understanding of the specific functions of PARP-1 and PARP-2.

While studies have linked both PARP-1 and PARP-2 with PCa development and progression, the distinct roles of PARP-1 vs. PARP-2 remain unclear. It was reported that PARP-1 and the catalytic subunit of DNA-dependent protein kinase (DNA-PKcs) interact with TMPRSS2:ERG gene fusion, which is required for ERG-mediated transcription and cell invasion in PCa (24). Beyond DNA-repair function, PARP-1 was found to play a role in regulating AR target genes by promoting AR recruitment to the promoters of its target genes (25). A recent study also showed that PARP1 and PARP2 are involved in AR variant driven transcription in CRPC cells (26). In a genetic epidemiological study, we explored genetic signatures that predispose patients to aggressive PCa and revealed a link between genetic variants in DNA-repair genes (including notably PARP-2) and aggressiveness of PCa (27). This led us to study the role of PARP-2 in PCa oncogenesis. In the present study, we have discovered a functional connection between

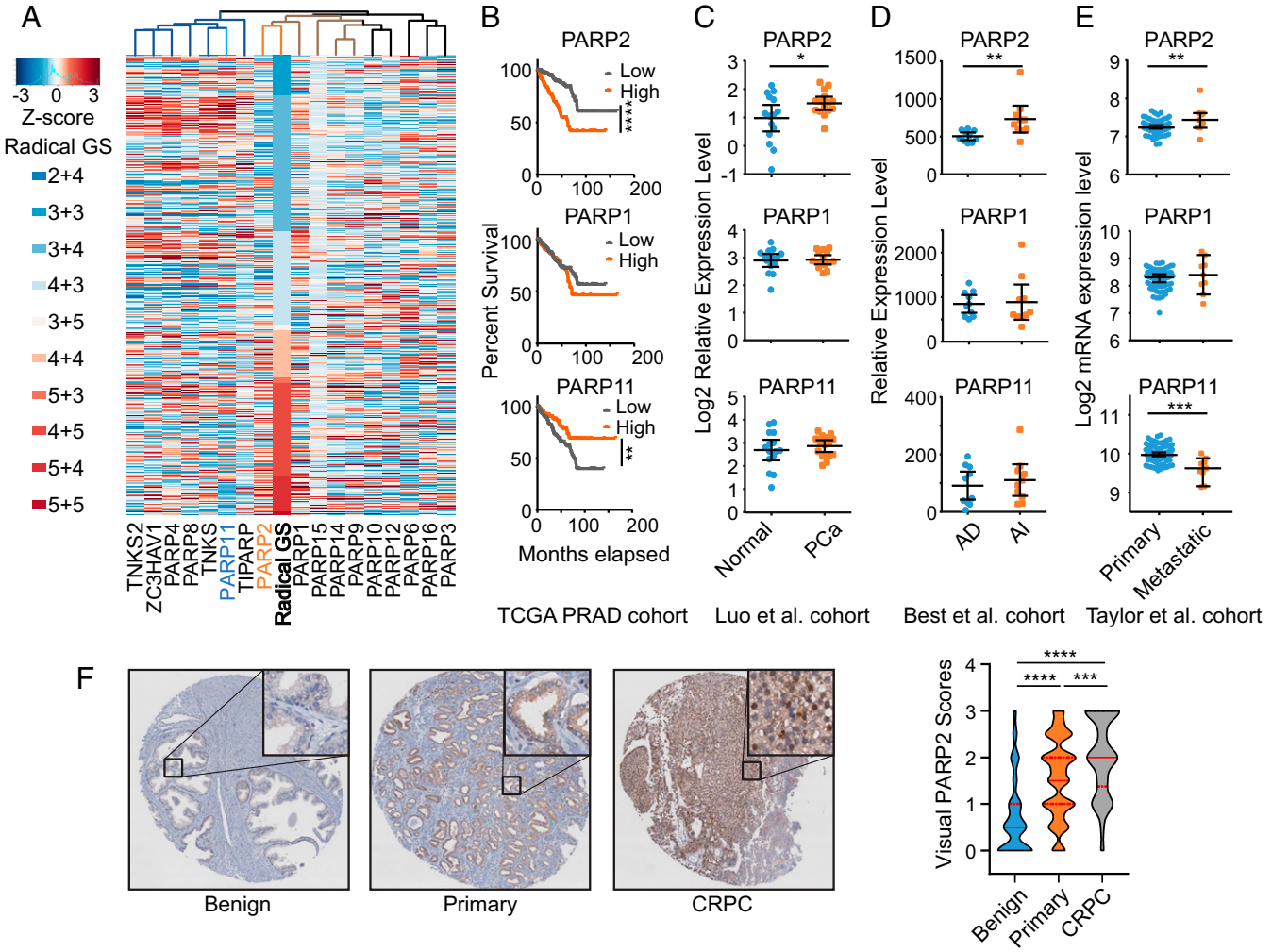

Fig. 1. PARP-2 is overexpressed in PCa. (*A*) Association of the mRNA expression of PARP family members with PCa radical prostatectomy Gleason score (GS) in TCGA dataset ($n = 499$). Each row represents an individual tumor sorted by GS. The gene expression levels are presented by Z-score values. (*B*) Kaplan—Meier plot of biochemical recurrence-free survival proportion of all patients in TCGA dataset with low ($n = 245$) or high ($n = 246$) expression levels of PARP-1, PARP-2, and PARP-11. (*C–E*) The relative mRNA expression levels of PARP-1, PARP-2, and PARP-11 in normal prostate tissues ($n = 15$) vs. PCa tumors ($n = 15$); androgen-dependent (AD) ($n = 10$) vs. androgen-independent (AI) ($n = 10$) tumors; and primary ($n = 76$) vs. metastatic ($n = 9$) tumors. Data represent mean ± 95% CI. (*F*) immunohistochemistry (IHC) analysis of PARP-2 protein expression on tissue microarrays (TMAs) composed of benign prostate tissues ($n = 232$), primary PCa ($n = 819$), and CRPC ($n = 78$) tumor cores. Representative IHC images (original magnification 4×; *Insets*, original magnification 20×) are presented (*Left*). The expression levels of PARP-2 were quantified by visual scoring and shown in a violin plot (*Right*). Red solid lines represent the median, and dashed lines are the 25th and 75th percentile. Statistical significance was determined by Kruskal–Wallis test followed by Tukey's test. *$P < 0.05$; **$P < 0.01$; ***$P < 0.001$; ****$P < 0.0001$.

PARP-2, AR, and FOXA1 in PCa cells. We demonstrate that PARP-2 is a key component in AR-mediated transcription through interacting with the pioneer factor FOXA1 and is required for PCa growth.

Results

Overexpression of PARP-2 Is Associated with PCa Aggressiveness. To explore the role of PARP proteins in PCa oncogenesis, we performed a metaanalysis on the mRNA expression levels of all 17 PARP members in primary PCa tumor samples from The Cancer Genome Atlas (TCGA) dataset (28). An unsupervised hierarchical clustering analysis showed that the expression of PARP-2 had the highest correlation with radical prostatectomy Gleason scores (R = 0.382, P = 1.07e−18) (Fig. 1*A*), followed by the expression of PARP-1 (R = 0.201, P = 6.09e−6). Interestingly, the expression of PARP-11 (R = −0.227, P = 3.02e−7) had a negative correlation with the aggressiveness of PCa. Survival analysis showed that overexpression of PARP-2, but not PARP-1, was significantly associated with PCa biochemical recurrence (Fig. 1*B*). In contrast, overexpression of PARP-11 was significantly associated with a better clinical outcome, indicating a tumor-suppressing role. In line with TCGA data, the PARP-2 mRNA levels were significantly elevated in PCa tumors compared with normal controls and further increased in androgen-independent primary tumors and in metastatic tumors using several publicly available PCa datasets (Fig. 1 *C*–*E*) (29–31). We further applied immunohistochemistry (IHC) assays to measure PARP-2 protein expression in a set of PCa tissue microarrays (TMAs) containing 1,129 tissue cores (Fig. 1*F* and *SI Appendix*, Fig. S1). Significantly higher PARP-2 protein expression was observed in primary PCa tumors compared with benign prostate tissues. While the PARP-2 protein levels were relatively similar between various Gleason groups among primary PCa tumors, we found much higher signal intensity of PARP-2 in the CRPC group. These results strongly support that PARP-2 plays an important role in PCa transformation and progression in contrast to other PARP members.

PARP-2 Is Required for the Growth of PCa Cells In Vitro and In Vivo. Next, we assessed the impact of PARP-2 on the growth of four PCa cell lines in comparison with PARP-1 using genetic approaches. Transient siRNA knockdown (KD) of either PARP-1 or PARP-2 markedly suppressed the growth of AR-positive LNCaP and VCaP cells but had a limited effect on AR-negative DU145 and PC-3 cells (Fig. 2*A*). We then established PARP-1 and PARP-2 knockout (KO) LNCaP cell lines using clustered regularly interspaced short palindromic repeats/CRISPR-associated protein 9 (CRISPR/Cas9) gene editing. Consistently, KO of PARP-1 or PARP-2 significantly inhibited LNCaP cell growth (Fig. 2*B*). This was further confirmed in colony formation assays (*SI Appendix*, Fig. S2). In addition, the loss of PARP-1 or PARP-2 in LNCaP cells evidently decreased their anchorage-independent growth (Fig. 2 *C* and *D*). We observed a greater inhibitory effect from PARP-2 KD compared with PARP-1 KD using gene-specific siRNAs. To determine the oncogenic role of PARP-2 in vivo, we implanted the PARP-1 and PARP-2 KO LNCaP cell lines subcutaneously (s.c.) into immunodeficient mice and found that depletion of either PARP-1 or PARP-2 gene completely diminished tumorigenic potential of LNCaP cells (Fig. 2*E*).

PARP-2 Is Critical for AR-Mediated Transcription. Although PARP-1 and PARP-2 account for ∼90% and ∼10% of total cellular enzymatic activity (or PARylation), respectively (14, 15), depletion of PARP-2 had comparable inhibitory effects, if not better, on LNCaP and VCaP cell growth in contrast to depletion of PARP-1. The inconsistency between their biological outcomes and enzymatic activity suggested that PARP-2 acts in a way distinct from PARP-1. To reconcile the mechanistic differences between these two proteins, we analyzed global gene expression changes after PARP-1 and PARP-2 KD in LNCaP cells using RNA-sequencing (RNA-seq). As shown in the volcano plot, well-characterized AR target genes, such as KLK2, KLK3/PSA, FKBP5, and TMPRSS2, topped the genes that were significantly suppressed after PARP-2 but not PARP-1 KD (Fig. 3*A*). We defined PARP-1– and PARP-2–regulated genes, respectively, by overlapping the differentially expressed genes generated from two independent siRNAs (Fig. 3*B*) (Dataset S1). Only a small fraction of genes were coregulated by both PARP-1 and PARP-2.

We next examined gene expression signatures enriched in PARP-1– or PARP-2–regulated genes using the Molecular Signature Database (MSigDB) (32, 33). Using "Hallmark" gene signatures, we revealed a significant enrichment of "UV-response" and "p53" pathway genes in PARP-1–regulated genes (Fig. 3*C*),

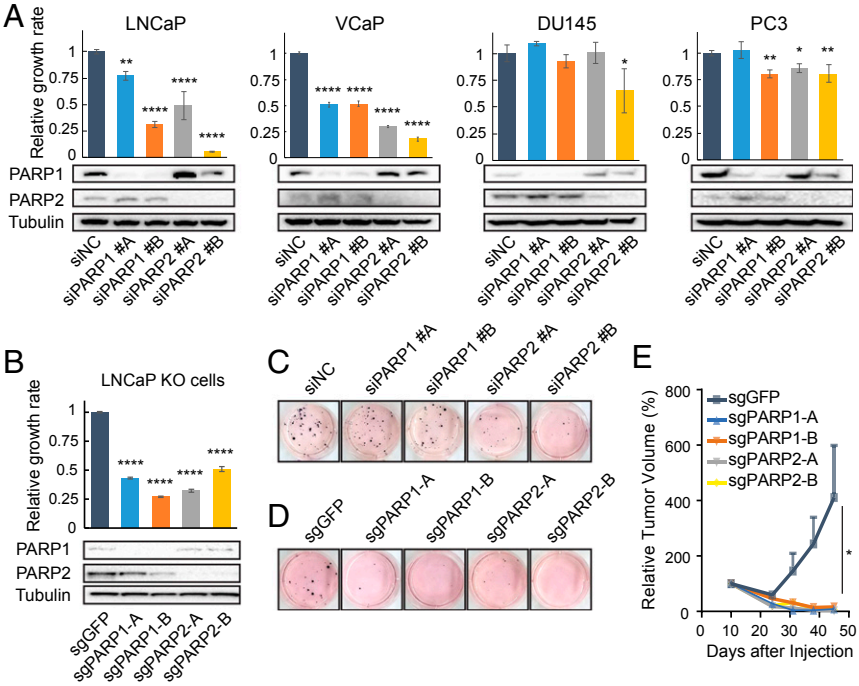

Fig. 2. PARP-2 is required for PCa growth. (*A*) Relative growth rate of PCa cells transfected with two independent PARP-1 or PARP-2 siRNAs compared with nonspecific control (NC) siRNA (*Upper*). Gene knockdown (KD) efficiency was determined by Western blot (*Lower*). (*B*) Effect of PARP-1 or PARP-2 gene knockout (KO) on LNCaP cell proliferation using two independent sgRNAs (*Upper*). Gene KO was confirmed by Western blot (*Lower*). (*C*) Anchorage-independent growth of LNCaP cells after PARP-1 or PARP-2 KD. (*D*) Anchorage-independent growth of LNCaP cells after PARP-1 or PARP-2 KO. (*E*) Relative tumor volume of PARP-1 and PARP-2 KO LNCaP xenografts in vivo (10 mice per group). The GFP KO LNCaP cell line was used as a control. All data represent the mean ± SD. Statistical significance was determined by one-way ANOVA followed by Tukey's multiple comparisons to the control group. *P < 0.05; **P < 0.01; ****P < 0.0001.

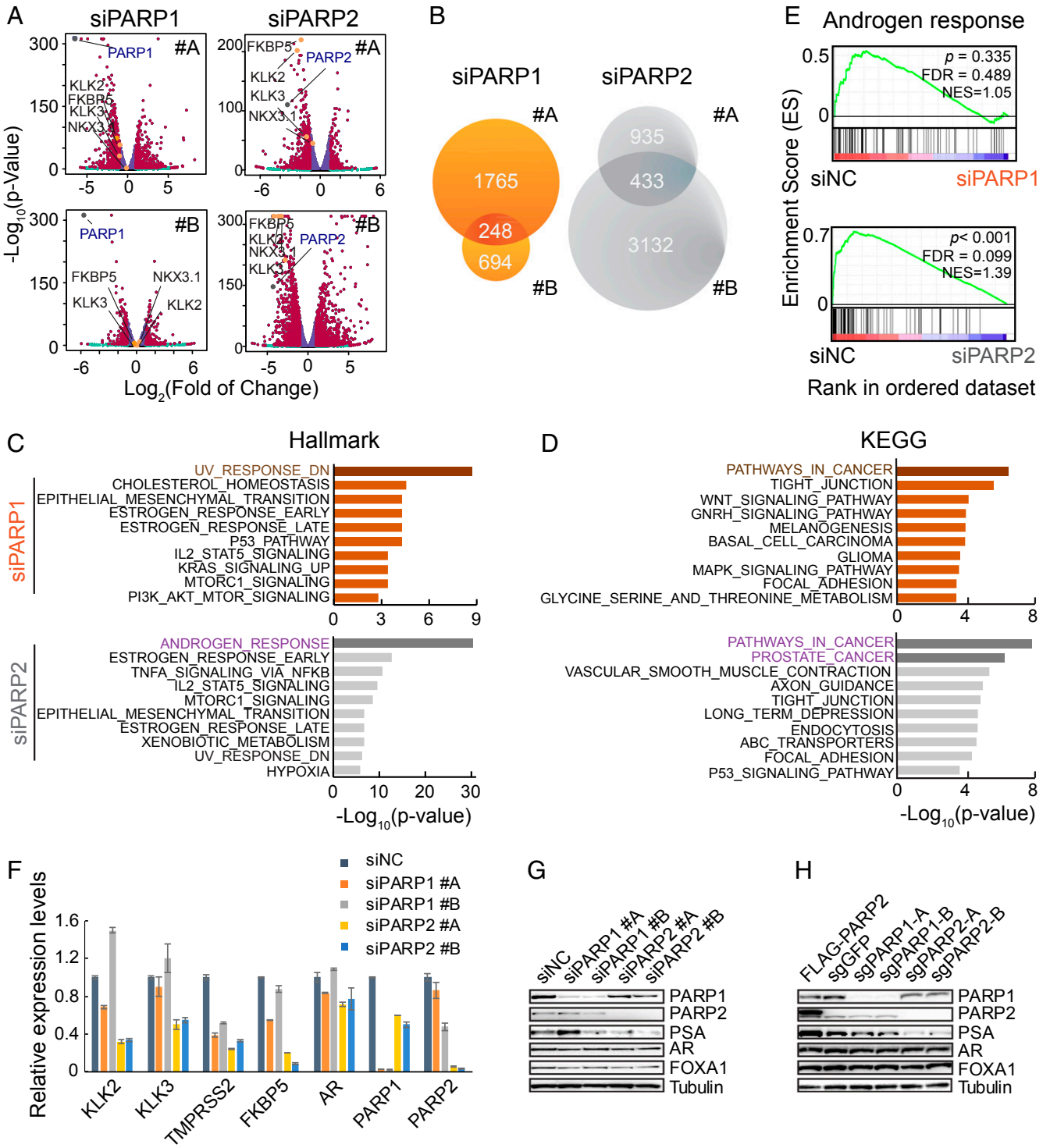

Fig. 3. PARP-2 is critical for AR-mediated transcription. (*A*) Gene expression profiling of LNCaP cells after PARP-1 or PARP-2 siRNA KD for 72 h with two independent siRNAs. Differentially expressed genes with fold change >1.75 and FDR <0.01 are labeled in red; four classic AR target genes are highlighted in orange; PARP-1 and PARP-2 are marked in gray. (*B*) PARP-1– and PARP-2–regulated genes are identified by overlapping the differentially expressed genes generated from the two siRNAs. (*C*) Enrichment of Hallmark signatures for PARP-1– and PARP-2–regulated genes. (*D*) Enrichment of KEGG signatures for PARP-1– and PARP-2–regulated genes. (*E*) GSEA of RNA-seq data showing enrichment of androgen response gene signature in PARP-1 or PARP-2 KD LNCaP cells. (*F*) Relative mRNA expression levels were determined by RT-qPCR in LNCaP cells transfected with either PARP-1 or PARP-2 siRNAs compared with nonspecific control (NC) siRNA. The mRNA expression data represent the mean ± SD of three technical replicates. (*G* and *H*) Western blot analyses depict protein levels of genes as indicated in PARP-1 and PARP-2 KD (*G*) or KO (*H*) LNCaP cells. The tubulin level serves as a protein loading control. All experiments except the RNA-seq were repeated at least three times.

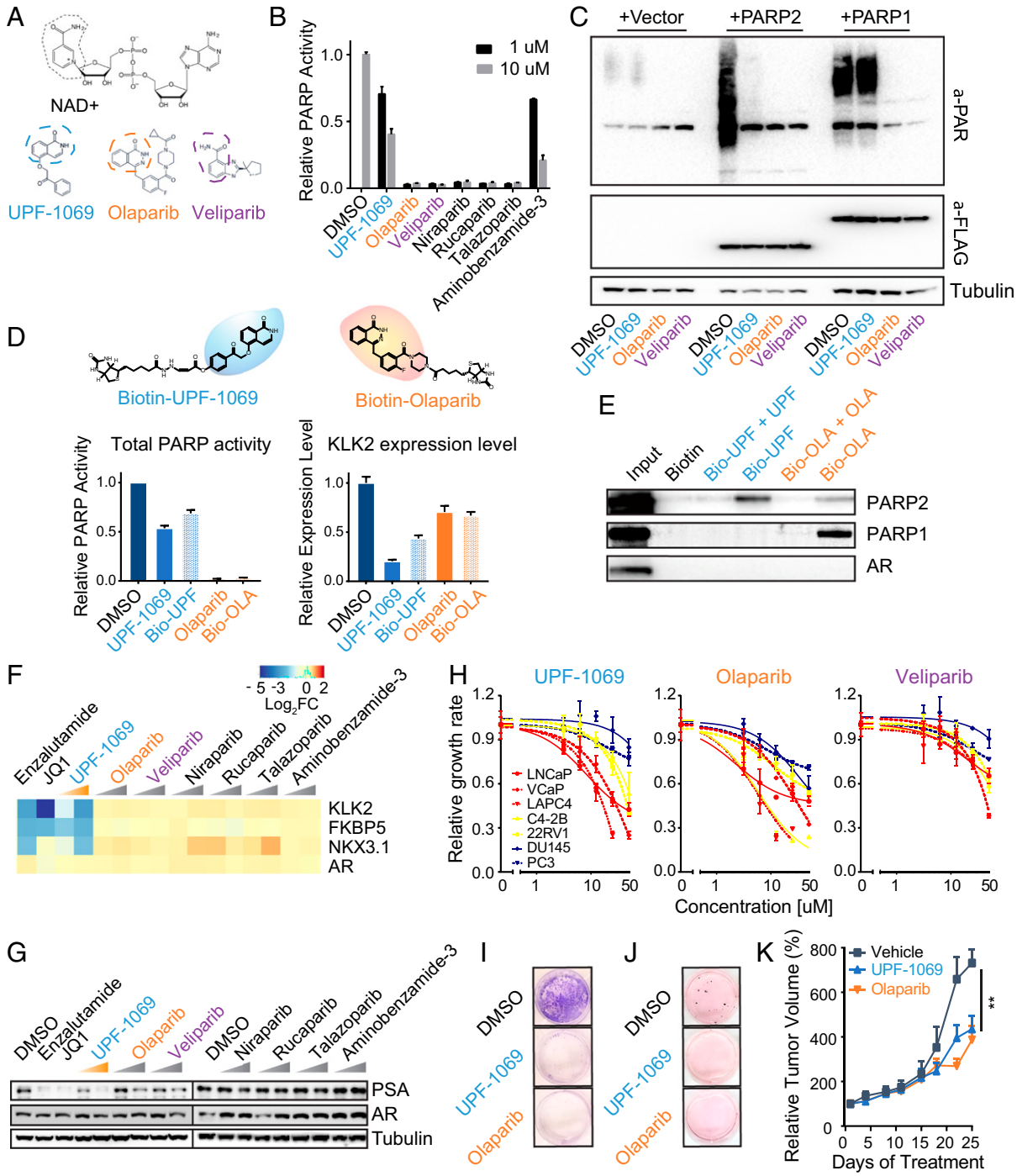

Fig. 4. Selective PARP-2 inhibitor UPF-1069 suppresses AR target gene expression and AR-positive PCa cell growth. (*A*) Chemical structures of NAD^+, UPF-1069, olaparib, and veliparib. Similar moieties shared by the compounds are circled. (*B*) LNCaP cells were treated with PARPi as indicated. Total PARP activity in cell lysates after the treatment was determined by PARP Universal Colorimetric Assay. (*C*) LNCaP cells were transfected with vector, FLAG-tagged PARP-1, or PARP-2 for 48 h before being treated with PARPi (10 μM) as indicated for another 4 h. The expression level of total PARylated proteins in cell lysates was determined by Western blot using antibody against poly(ADP-ribose) (PAR). Anti-FLAG was used to determine the expression levels of PARP-1 and PARP-2. The tubulin level serves as a protein loading control. (*D*) Synthesis of biotinylated UPF-1069 and olaparib. (*Upper*) The chemical structures of biotinylated small molecules with UPF-1069 and olaparib highlighted in blue and orange, respectively. The efficacy of biotinylated UPF-1069 (Bio-UPF) and olaparib (Bio-OLA), in comparison with unmodified PARPi, was determined by their inhibitory effects on total PARP activity (*Lower Left*) and KLK2 expression levels (*Lower Right*) after treatment for 24 h. (*E*) Western blot analyses of protein eluates from biotinylated UPF-1069 or olaparib coated beads after incubation with LNCaP cell lysate in the presence or absence of unmodified UPF-1069 and olaparib. (*F*) A heat map shows expression alteration of AR and AR target genes in LNCaP cells after treatment with Enzalutamide (10 μM), JQ1 (0.5 μM), or PARPi (1 and 10 μM) for 24 h. (*G*) Protein expression levels of PSA, AR, and tubulin in LNCaP cells after treatment with small molecule inhibitors as indicated for 24 h. (*H*) Inhibition of PCa cell proliferation by UPF-1069, olaparib, and veliparib. Red curves, androgen-dependent PCa cell lines; yellow, AR-positive CRPC cell lines; blue, AR-negative CRPC lines. (*I* and *J*) Clone-forming ability of LNCaP cells after treatment with UPF-1069 (10 μM), olaparib (10 μM), or DMSO was determined by clonogenic assays (*I*) and soft agar assays (*J*). (*K*) Relative tumor volume of VCaP xenografts in mice treated with vehicle, UPF-1069 or Olaparib for 3.5 wk (7 mice per group). All experiments except for animal experiment were repeated at least three times. All data represent the mean ± SD. Statistical significance was determined by one-way ANOVA followed by Tukey's multiple comparisons to the control group. $^{**}P < 0.01$.

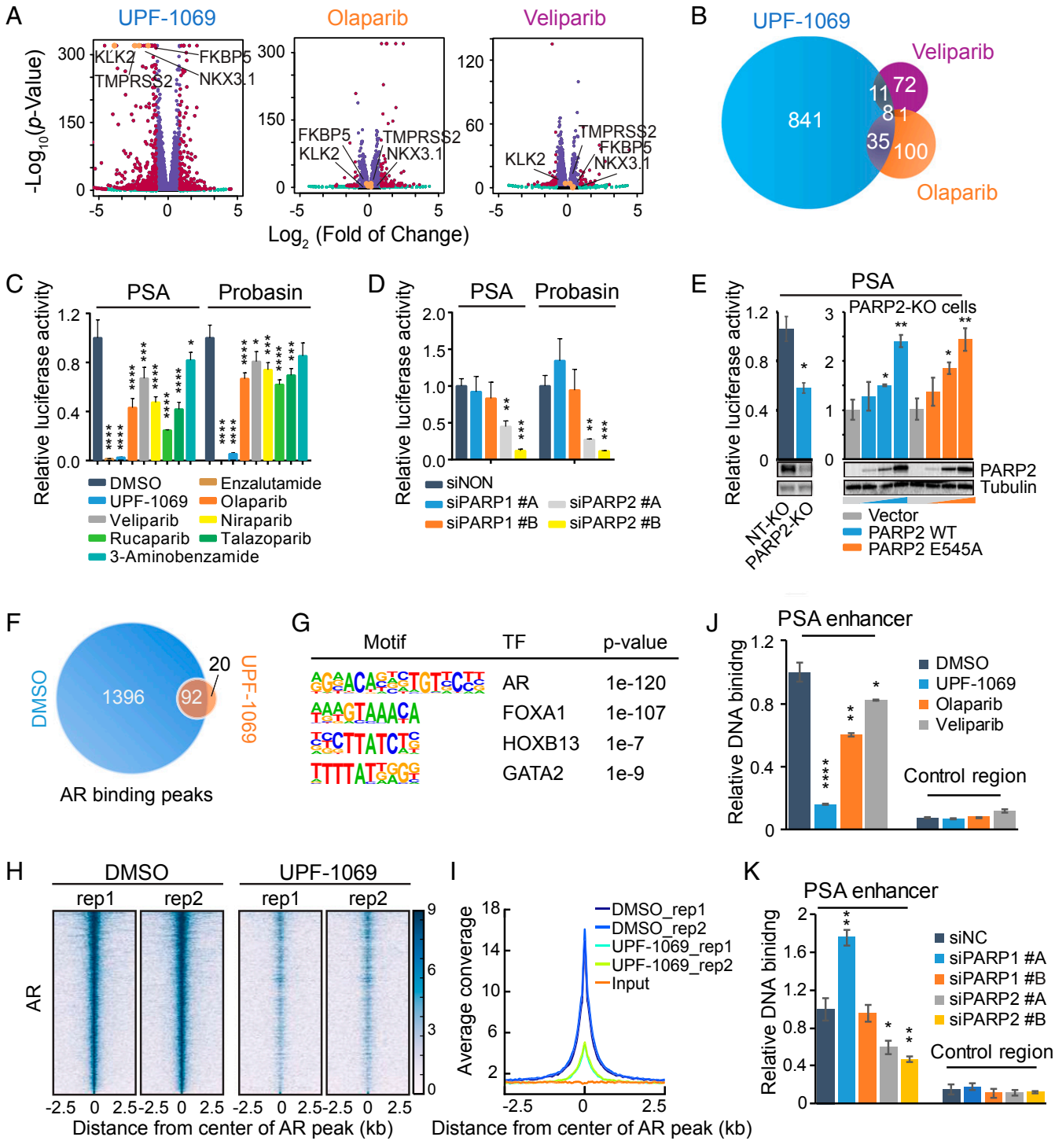

Fig. 5. Inhibition of PARP-2 abrogates genome-wide AR recruitment. (*A*) Gene expression profiling of LNCaP cells after treatment with UPF-1069 (10 μM), olaparib (10 μM), or veliparib (10 μM) for 24 h. Differentially expressed genes with fold change >2 and FDR <0.01 are labeled in red. Four classic AR target genes are highlighted in orange. (*B*) Overlap between UPF-1069–, olaparib-, and veliparib-altered genes. (*C*) PSA and Probasin luciferase reporter plasmids containing highly conserved androgen response elements were transfected into LNCaP cells. The treatment with PARPi (10 μM) as indicated started 4 h after transfection. Luciferase activity was measured 24 h after reporter transfection. (*D*) PARP-1 and PARP-2 siRNA KD was conducted in LNCaP cells through reverse transfection 48 h before luciferase reporter plasmid transfection. Luciferase activity was measured 24 h after reporter transfection. (*E*) A PARP-2 KO cell line and a nontargeting (NT) control line were generated through ribonucleoprotein (RNP) delivery approach as described in *Materials and Methods*. KO efficiency was confirmed by Western blot. PSA luciferase report activity was decreased in PARP-2 KO cells but rescued after overexpression of PARP-2 wild-type (WT) or E545A mutant plasmid in a dose-dependent manner (0, 50, 100, 200 ng per well). PARP-2 overexpression was examined by Western blot. (*F*) Venn diagram illustrating the overlap of AR binding sites identified by AR ChIP-seq in LNCaP cells between DMSO and UPF-1069 (10 μM) treatments for 16 h. (*G*) Motifs enriched in AR binding sites. (*H*) A heat map showing AR ChIP-seq signal density in a region of 2.5 kb flanking AR binding summits. Two replicates (rep) for each treatment are presented. (*I*) A summary plot of AR average signal density (reads per genomic coverage) across all AR-binding sites. (*J* and *K*) Relative AR binding determined by ChIP-qPCR at the PSA enhancer and the control region in LNCaP cells after treatment with PARPi for 16 h (*J*) or 2 d after siRNA KD (*K*). All data represent the mean ± SD of three technical replicates. All experiments except for RNA-seq and ChIP-seq were repeated at least three times. Statistical significance was determined by one-way ANOVA followed by Tukey's multiple comparisons to the control group. **P* < 0.05; ***P* < 0.01; ****P* < 0.001; *****P* < 0.0001.

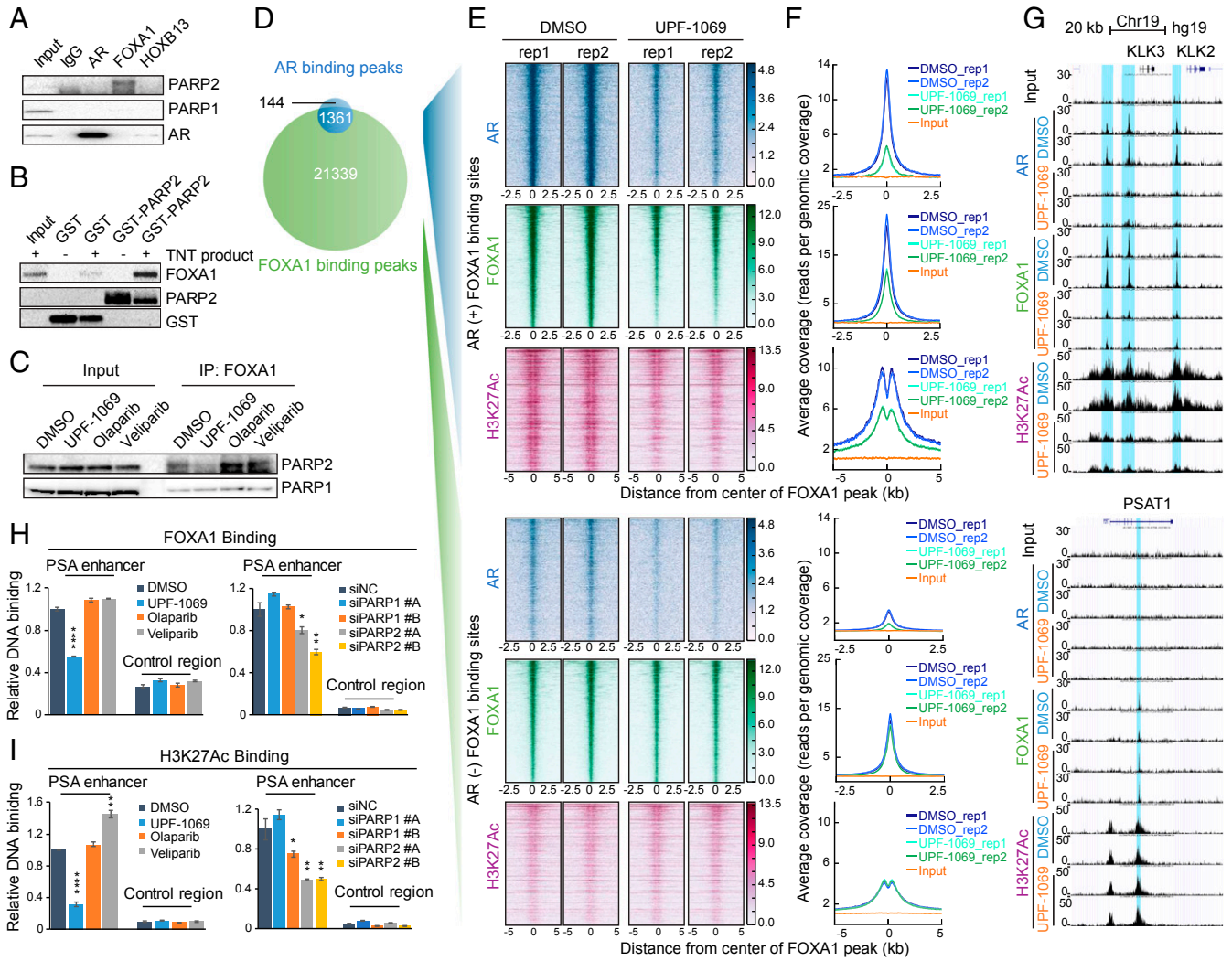

Fig. 6. PARP-2 modulates FOXA1 function. (*A*) Co-IP showing association of endogenous PARP-1/PARP-2 with AR/FOXA1/HOXB13 in LNCaP cells. (*B*) GST pull-down showing direct interaction between purified GST-PARP-2 protein and FLAG-FOXA1 in vitro translation product (TNT product). (*C*) Co-IP showing Interaction between PARP-1/PARP-2 and FOXA1 in LNCaP cells after treatment with PARPi (10 μM) for 6 h. (*D*) Venn diagram showing the overlap of AR and FOXA1 binding sites identified by ChIP-seq in LNCaP cells. (*E* and *F*) Inhibition of PARP-2 disrupts FOXA1 binding and function at AR binding sites. Heat maps (*E*) and average signal density plots (*F*) showing AR, FOXA1, and H3K27Ac binding at the AR-occupied (+) (*Upper*) and non-AR-occupied (–) (*Lower*) FOXA1 binding sites (2.5 kb flanking FOXA1 binding summits) after treatment with DMSO or UPF-1069 (10 μM) for 16 h. (*G*) AR, FOXA1, and H3K27Ac ChIP-seq signals at KLK2, KLK3, and PSAT1 loci. (*H* and *I*) ChIP-qPCR results showing FOXA1 (*H*) and H3K27Ac (*I*) binding at the PSA enhancer and the control region in LNCaP cells after treatment with PARPi as indicated or PARP-1/PARP-2 siRNA KD. All experiments except for ChIP-seq were repeated at least three times. The ChIP-qPCR data represent the mean ± SD of three technical replicates. Statistical significance was determined by one-way ANOVA followed by Tukey's multiple comparisons to the control group. $*P < 0.05$; $**P < 0.01$; $****P < 0.0001$.

which was consistent with the notion that PARP-1 is critical in repairing DNA damage and restoring genome stability. In contrast, PARP-2–regulated genes were primarily involved in androgen response. Overlapping with Kyoto Encyclopedia of Gene and Genomes (KEGG) gene sets showed that PARP-2–regulated genes were highly enriched in "prostate cancer" in particular (Fig. 3*D*). We further employed the gene set enrichment analysis (GSEA) using the "androgen response" signature and revealed significant repression of androgen-regulated genes in PARP-2 but not in PARP-1 KD cells (Fig. 3*E*). Using RT-qPCR, we confirmed that KD of PARP-2 markedly repressed the expression of AR target genes (KLK2, KLK3/PSA, TMPRSS2, and FKBP5) (Fig. 3*F*). KD of PARP-1 inhibited TMPRSS2 expression but had little effect on KLK2, KLK3/PSA, and FKBP5 expression. The protein level of PSA was also decreased after PARP-2 KD or KO (Fig. 3 *G* and *H*). Notably, AR expression remained unchanged, indicating that the suppression of AR target genes was not due to the alteration of AR expression. Interestingly, we found that dual KD of PARP-1 and PARP-2 did not affect the expression of AR target genes (*SI Appendix*, Fig. S3). This is likely because KD of PARP-1 predominantly induced p53-mediated cellular responses, which might overshadow the inhibitory effect on AR signaling by KD of PARP-2 at the same time. Taken together, our results suggest that PARP-2 is involved in PCa tumorigenesis, likely through transcriptionally modulating AR-mediated gene expression, which is functionally differentiated from the DNA damage repair protein PARP-1.

Selective PARP-2 Inhibitor UPF-1069 Suppresses the Expression of AR Target Genes. We then asked whether the PARPi could interfere with AR-mediated transcription as well. We assembled four FDA-approved PARPis (olaparib, niraparib, talazoparib, and rucaparib) and two PARPis under preclinical investigation (veliparib and 3-aminobenzamide). These pan-PARPis inhibit both PARP-1 and

PARP-2 enzymatic activity. In addition, we employed the compound UPF-1069, a selective PARP-2 inhibitor with ~27-fold selective over PARP-1 (34, 35). The structures of pan-PARPis (olaparib and veliparib) and selective PARP-2 inhibitor (UPF-1069) contain a key pharmacophore mimicking nicotinamide moiety that competes with NAD^+ (Fig. 4*A*). To assess the inhibitory potency of PARPi, we measured total PARP enzymatic activity from LNCaP whole cell lysates after treatment with PARPi using an in vitro PARP universal colorimetric assay. As expected, all pan-PARPis, except 3-aminobenzamide, completely abolished PARP activity (Fig. 4*B*). In contrast, UPF-1069 suppressed the total PARP activity down to 40% at 10 μM, suggesting that UPF-1069 is not a potent pan-PARPi. To determine the specificity of UPF-1069, we measured in vivo PARylation using antibody against poly(ADP-ribose). We detected modest levels of endogenous PARylation (largely attributed to PARP-1 activity) in LNCaP cells, which was abolished by olaparib and veliparib, but not by UPF-1069 (Fig. 4*C*). We then overexpressed PARP-1 and PARP-2 in LNCaP cells. We showed that UPF-1069 completely inhibited the PARP-2–induced PARylation but had no effect on PARP-1. In contrast, olaparib and veliparib completely blocked the PARylation derived from both PARP-1 and PARP-2. To further determine whether UPF-1069 specifically interacts with PARP-2, we linked UPF-1069 and olaparib with a biotin moiety to allow their application in a pull-down assay (*SI Appendix*, Fig. S4). Biotinylated UPF-1069 and olaparib have similar inhibitory effects on total PARP activity and AR target gene KLK2 expression compared with unmodified UPF-1069 and olaparib (Fig. 3*D*). Biotinylated UPF-1069 and olaparib were then immobilized on streptavidin beads and incubated with whole cell lysates extracted from LNCaP cells overexpressed with PARP-1 and PARP-2. As shown in the Western blot, UPF-1069 could selectively bind to PARP-2 (Fig. 4*E*). As a pan-PARPi, olaparib interacted with both PARP-1 and PARP-2 although the binding with PARP-2 was weaker than UPF-1069. These interactions were outcompeted by unmodified UPF-1069 and olaparib, respectively. Taken together, our data demonstrated UPF-1069 as a selective PARP-2 inhibitor.

Next, we examined the mRNA levels of three AR target genes (KLK2, FKBP5, and NKX3.1) in LNCaP cells treated with a panel of PARPis (Fig. 4*F*). As controls, enzalutamide (AR antagonist) and JQ1 (Bromodomain and Extra-Terminal motif [BET] inhibitor) (36) were included. Of all PARPis tested, only UPF-1069 significantly suppressed all three AR target genes in a dose-dependent manner. The PSA protein level was also significantly decreased after UPF-1069 treatment (Fig. 4*G*). Only minor or no effect was observed after treatment with other PARPis. Notably, PARPi did not change the expression of AR significantly, indicating that UPF-1069 does not regulate AR target genes through modulation of AR expression. In addition, we found that both olaparib and UPF-1069 had little effect on the expression and activity of SIRT1 (*SI Appendix*, Fig. S5), a NAD^+-dependent enzyme, which is regulated by PARP-2 as previously reported (22). Thus, the inhibition of AR target gene expression by UPF-1069 cannot be attributed to its impact on NAD^+ bioavailability and SIRT1 transcription in PCa cells.

UPF-1069 Inhibits PCa Cell Growth In Vitro and In Vivo. To determine whether UPF-1069 can inhibit PCa cell growth, we performed cell proliferation assays on a panel of seven PCa cell lines (Fig. 4*H*). We found that UPF-1069 inhibited the growth of both androgen-dependent PCa cells (LAPC4, LNCaP, and VCaP) and AR-positive CRPC cells (C4-2B and 22RV-1) although androgen-dependent PCa cells showed greater sensitivity. In contrast, AR-negative CRPC cells (PC3 and DU145) showed resistance. No clear pattern was noticeable after treatment with olaparib or veliparib although PCa cells were more sensitive to olaparib than veliparib, indicating differential efficacy between PARPis even with similar catalytic inhibitory potency. Moreover, UPF-1069 and olaparib markedly suppressed the colony formation and anchorage-independent growth of LNCaP cells (Fig. 4 *I* and *J*). In agreement with in vitro proliferation results, UPF-1069 significantly inhibited VCaP tumor growth in vivo (Fig. 4*K*). No weight loss was observed in UPF-1069–treated mice (*SI Appendix*, Fig. S6). Similar tumor suppression was also achieved with olaparib treatment. Our data indicate that selective targeting of PARP-2 with a pharmacological agent is sufficient to suppress PCa growth in preclinical models.

UPF-1069 Abrogates AR Transcriptional Activity in PCa Cells. To explore the molecular mechanism by which PARPis suppress PCa cell growth, we analyzed the global gene expression changes in LNCaP cells after treatment with UPF-1069, olaparib, and veliparib using RNA-seq. As shown in the volcano plot (Fig. 5*A*), UFP-1069 had a much greater effect on gene expression (895 differentially expressed genes) compared with olaparib (144 genes) and veliparib (92 genes) (Dataset S1). In accordance with PARP-2 KD results, pharmaceutical inhibition of PARP-2 dramatically altered AR-mediated gene expression, with classical AR target genes (KLK2, KLK3/PSA, FKBP5, NKX3.1, and TMPRSS2) being on the top of the differentially expressed gene list. However, broadly quenching PARP activity using either olaparib or veliparib was not able to affect these genes. Only a small number of commonly altered genes were identified between three different treatments (Fig. 5*B*). Analyses of MSigDB showed that UPF-1069–altered genes were highly enriched for "androgen response" hallmark while olaparib-altered genes were involved in "p53" and "apoptosis" pathways (*SI Appendix*, Fig. S7).

To further examine the impact of PARPi on AR activity, we performed androgen response element driven luciferase report assays and showed that UPF-1069 completely abolished the PSA and Probasin reporter activity while pan-PARPis had a minor to moderate effect (Fig. 5*C*). Interestingly, pan-PARPis showed a similar inhibition on WNT and E2F signaling (*SI Appendix*, Fig. S8), indicating a general effect on transcriptional regulation. Consistently, the PSA and Probasin reporter activity was significantly inhibited after PARP-2 KD (Fig. 5*D*) while KD of PARP-1 had no effect. Furthermore, we generated a PARP-2 KO LNCaP cell line through a Ribonucleoprotein (RNP) delivery approach, which has no DNA integration into the genome and fewer off-target effects. We found that the PSA reporter activity was significantly decreased in PARP-2 KO cells compared with nontarget (NT) control cells (Fig. 5*E*). Notably, both wild-type PARP-2 and enzymatically inactive E545A mutant PARP-2 (*SI Appendix*, Fig. S9) could restore the PSA reporter activity, indicating that PARP-2 enzymatic activity is not required for modulating AR transcriptional activity. Taken together, our data suggest that UPF-1069 suppresses PCa cell growth by attenuating AR signaling while olaparib induces p53-dependent apoptosis to achieve a similar effect. Importantly, the effect of PARPis on gene expression is not correlated with their inhibitory potency on PARP enzymatic activity.

Inhibition of PARP-2 Attenuates Genome-Wide AR Recruitment. We then asked whether inhibition of PARP-2 by UPF-1069 affects AR binding to the genome. We performed chromatin immunoprecipitation-sequencing (ChIP-seq) with an antibody against AR in LNCaP cells. Surprisingly, the number of AR binding peaks identified after UPF-1069 treatment dramatically decreased (Fig. 5*F*). As expected, all AR binding peaks were enriched with AR and its coregulator (FOXA1, HOXB13, and GATA2) motifs (Fig. 5*G*). In line with the global effect of UPF-1069 on AR-mediated gene expression, a striking reduction of global AR binding was observed (Fig. 5 *H* and *I*). ChIP-qPCR assays confirmed that AR binding was diminished by UPF-1069 and less so by olaparib and veliparib at the PSA (Fig. 5*J*) and other AR-targeted loci (*SI Appendix*, Fig. S10). KD of PARP-2 also attenuated AR binding, supporting that AR binding is largely modulated by PARP-2 but not PARP-1 (Fig. 5*K* and *SI Appendix*, Fig. S10).

PARP-2 Modulates the Pioneer Factor FOXA1 Function. Given the genome-wide regulatory effect of PARP-2 on AR occupancy, we hypothesized that PARP-2 may physically interact with AR and function as a coactivator. We performed a coimmunoprecipitation (Co-IP) assay in LNCaP cells. Surprisingly, no interaction

was detected between AR and either PARP-1 or PARP-2 (Fig. 6*A*). Instead, we observed that the pioneer factor FOXA1 strongly interacted with PARP-2 but not with PARP-1. Neither PARP-1 nor PARP-2 could bind to HOXB13, another critical AR coregulator (37). Using an in vitro GST pull-down assay, we further demonstrated that PARP-2 directly interacted with FOXA1 (Fig. 6*B*). However, FOXA1 was not modified or PARylated by PARP-2 (*SI Appendix*, Fig. S11). Instead, we found that both wild-type and E545A mutant PARP-2 could interact with FOXA1 (*SI Appendix*, Fig. S12), in line with the notion that PARP-2 modulates AR activity through interacting with FOXA1 independent of its enzymatic activity. Importantly, the interaction between PARP-2 and FOXA1 could be blocked by UPF-1069 (Fig. 6*C*). Interestingly, pan-PARPis seem to enhance the PARP-2/FOXA1 interaction, likely due to PARP trapping to chromatin induced by pan-PARPi (38).

We then tested whether selective inhibition of PARP-2 could impair the FOXA1 chromatin association and function. We employed ChIP-seq with antibodies against FOXA1 and an enhancer histone mark, histone H3 lysine 27 acetylation (H3K27Ac), in LNCaP cells after treatment with UPF-1069. In agreement with previous studies (5, 37), AR binding sites were largely overlapped with FOXA1 binding sites (>90%) (Fig. 6*D*). We divided FOXA1 binding sites into two groups, AR-occupied and non–AR-occupied regions. Strikingly, UPF-1069 treatment not only abrogated AR recruitment but also diminished FOXA1 binding in the AR-occupied regions (Fig. 6 *E*–*G*). Accordingly, H3K27Ac was also decreased within these regions, suggesting impaired enhancer activity. These changes were not observed in the non–AR-occupied FOXA1 binding sites. ChIP-seq results were further validated by ChIP-qPCR at the PSA enhancer (Fig. 6 *H* and *I*). In agreement with pharmaceutical inhibition, KD of PARP-2 also led to a reduction of FOXA1 and H3K27Ac binding to the PSA enhancer. KD of PARP-1, however, showed no effect on FOXA1 binding and a mild H3K27Ac decrease by only one of the siRNAs. Taken together, our findings suggest that inhibition of PARP-2 disrupts FOXA1 binding and function at the AR enhancers, which in turn attenuates AR-mediated transcription (Fig. 7).

Discussion

Understanding the mechanisms underlying AR-mediated transcription is a critical step for the development of effective therapies for PCa. In the present study, we have identified PARP-2 as an oncogenic contributor to AR signaling through interacting with FOXA1 at prostate-specific enhancers, thereafter promoting PCa growth. Our findings offer a mechanistic insight into PARP-2 as a potential therapeutic target and shed light on a selective PARP-2 inhibitor in the treatment of PCa.

While we have demonstrated that both PARP-1 and PARP-2 are required for PCa cell growth, our analyses reveal that genetic and pharmacological inhibition of PARP-1 alters gene expression implicated in p53-mediated cellular response and apoptosis. In contrast, inhibition of PARP-2 has a significant impact on AR-mediated gene expression, which is comparable with enzalutamide treatment. It should be noted that PARP-1 is generally involved in the interplay between transcription and DNA repair since transcription has classically been considered a danger to genome integrity (39). As AR action has been linked to DNA damage and associated response (40, 41), it is not surprising that the high-abundant protein PARP-1 may somewhat interact with AR (42) or be considered as a coactivator (25). Moreover, studies have shown that the association between FOXA1 and DNA-repair complex is critical for the transcription pioneering and epigenetic reprogramming (43). Thus, it is expected that inhibition of PARP-1 may affect AR-mediated transfection to a certain extent. Nevertheless, PARP-1 likely impacts transcriptional regulation in a more ubiquitous fashion while PARP-2 is a critical component in AR signaling specifically. The oncogenic role of PARP-2 in PCa is further supported by the finding that PARP-2 is overexpressed in primary PCa and more so in CRPC tumors. Interestingly, PARP-2 is highly expressed in normal testicular tissues. KO of PARP-2 but not PARP-1 causes defect of spermatogenesis in mice (17), which is the same phenotype observed when AR is knocked out, supporting a specific role of PARP-2 in AR signaling.

Current clinically used PARPi abolishes both PARP-1 and PARP-2 catalytic activity, which raises the question of why these pan-PARPis (such as olaparib) have a limited effect on AR signaling in contrast to the selective PARP-2 inhibitor UPF-1069. Studies have shown that the efficacy of PARPis does not always rely on their catalytic inhibitory potency. For example, trapping PARP-1 and PARP-2 onto damaged DNA has been correlated with the cytotoxicity of PARPi (38), and yet PARPis with equal catalytic inhibitory potency show markedly different PARP trapping ability and cytotoxicity. Furthermore, catalytic-independent functions for both PARP-1 and PARP-2 have been reported (44, 45). Indeed, our results support the notion that PARP-2 enzymatic activity is not required for its role in AR-mediated transcription. Thus, blocking PARP-2 enzymatic activity by pan-PARPi is neither sufficient nor necessary for AR inhibition. We reason that UPF-1069 inhibits PARP-2 and abolishes AR activity, likely through its unique physicochemical properties, despite its relatively weak catalytic inhibition. We have provided compelling evidence that UPF-1069 strongly interacts with PARP-2 and disrupts the interaction between PARP-2 and FOXA1, which in turn attenuates AR recruitment. This cannot be achieved by pan-PARPi. Although efforts were made in this study to prove UPF-1069 as a selective PARP-2 inhibitor, we cannot rule out the possibility that UPF-1069 may interact with other proteins, including other PARP members. Proteome-wide profiling study has revealed PARPis to have compound-specific secondary targets, which may be involved in the therapeutic effects of these drugs (46). Considerable variability has been reported between different PARPis in the clinical

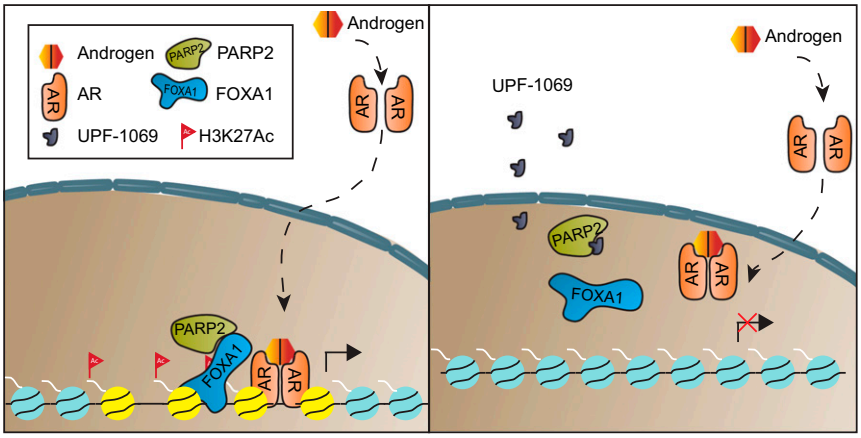

Fig. 7. Model depicting the mechanism by which selective targeting of PARP-2 attenuates AR signaling and inhibits PCa growth. PARP-2 enhances AR transcriptional activity via physically interacting with the pioneer factor FOXA1. Selective PARP-2 inhibitor UPF-1069 blocks this interaction, diminishes the genomic occupancies of FOXA1 and H3K27Ac at AR binding sites, and, thereby, inhibits AR-mediated gene expression and PCa growth.

development despite similar catalytic inhibition (47). Further investigation is necessary to explore other UPF-1069–associated proteins and potential off-target effects using proteomic approaches. Mechanistic characterization of each PARPi may guide a better application of these drugs under different disease settings.

PCa patients may benefit from selective targeting of PARP-2. First, pan-inhibitors normally have more side effects than selective inhibitors. As expression profiling indicates that PARP-11 may play a tumor-suppressive role in PCa development and progression, inhibition of total PARP activity may in fact denote unfavorable outcomes. Studies have even shown that inactivation of PARP-1 by gene-targeted deletion may lead to epithelial-mesenchymal transition induction toward high-grade prostate tumors (48), which may not be beneficial to patients in certain disease contexts. Second, the therapeutic outcomes of current pan-PARPis rely on whether tumors have HR deficiency. Lack of biomarkers for patient selection and quickly developed drug resistance are the major obstacles. Selective targeting of PARP-2 through the FOXA1/AR pathway may broaden the clinical application of PARP-targeted therapy in PCa management without considering HR deficiency status. Finally, selective targeting of PARP-2 may potentially provide an alternative therapeutic strategy for AR inhibition through disrupting FOXA1 binding instead of targeting AR directly.

Materials and Methods

Cell Lines and Materials. Prostate cancer cell lines were maintained in RPMI 1640 (for LNCaP, LAPC4, C4-2B, 22Rv1, PC-3, and DU145) or DMEM (for VCaP) supplemented with 10% FBS as previously described (49). The 293T cells were obtained from ATCC and maintained in DMEM with 10% FBS. All cell lines were authenticated using high-resolution small tandem repeats (STRs) profiling at Dana-Farber Cancer Institute (DFCI) Molecular Diagnostics Core Laboratory and were confirmed *Mycoplasma*-free before experiments. The small molecule inhibitors, antibodies, siRNAs, sgRNAs, and PCR primers are listed in *SI Appendix*, Table S1.

Statistical Analyses. Quantitative measurements are graphed as mean ± SD from at least three biological replicates unless otherwise indicated. All analyses were carried out using Prism software (GraphPad). One-way ANOVA (or Kruskal–Wallis test) followed by post hoc Tukey's test was used to calculate significance using $P < 0.05$.

Other Methods are described in *SI Appendix*, *Supplementary Materials and Methods*. ChIP-seq and RNA-seq data have been deposited into the Gene Expression Omnibus (GEO) database (accession no. GSE114275).

ACKNOWLEDGMENTS. We thank Quang-De Nguyen, Kristen L. Jones, Rebecca J. Modiste, and Ruthie Jia for technical support in this study. This work was supported by Department of Defense Idea Award Grant W81XWH-17-1-0251 (to L.J.).

1. J. S. de Bono *et al*.; COU-AA-301 Investigators, Abiraterone and increased survival in metastatic prostate cancer. *N. Engl. J. Med.* **364**, 1995–2005 (2011).
2. H. I. Scher *et al*.; AFFIRM Investigators, Increased survival with enzalutamide in prostate cancer after chemotherapy. *N. Engl. J. Med.* **367**, 1187–1197 (2012).
3. D. J. Crona, Y. E. Whang, Androgen receptor-dependent and -independent mechanisms involved in prostate cancer therapy resistance. *Cancers (Basel)* **9**, E67 (2017).
4. Y. A. Yang, J. Yu, Current perspectives on FOXA1 regulation of androgen receptor signaling and prostate cancer. *Genes Dis.* **2**, 144–151 (2015).
5. B. Sahu *et al*., Dual role of FoxA1 in androgen receptor binding to chromatin, androgen signalling and prostate cancer. *EMBO J.* **30**, 3962–3976 (2011).
6. H. J. Jin, J. C. Zhao, L. Wu, J. Kim, J. Yu, Cooperativity and equilibrium with FOXA1 define the androgen receptor transcriptional program. *Nat. Commun.* **5**, 3972 (2014).
7. C. E. Barbieri *et al*., Exome sequencing identifies recurrent SPOP, FOXA1 and MED12 mutations in prostate cancer. *Nat. Genet.* **44**, 685–689 (2012).
8. D. C. Wedge *et al*.; CAMCAP Study Group; TCGA Consortium, Sequencing of prostate cancers identifies new cancer genes, routes of progression and drug targets. *Nat. Genet.* **50**, 682–692 (2018).
9. W. L. Kraus, PARPs and ADP-ribosylation: 50 years . . . and counting. *Mol. Cell* **58**, 902–910 (2015).
10. H. E. Bryant *et al*., Specific killing of BRCA2-deficient tumours with inhibitors of poly(ADP-ribose) polymerase. *Nature* **434**, 913–917 (2005).
11. H. Farmer *et al*., Targeting the DNA repair defect in BRCA mutant cells as a therapeutic strategy. *Nature* **434**, 917–921 (2005).
12. J. Mateo *et al*., DNA-repair defects and olaparib in metastatic prostate cancer. *N. Engl. J. Med.* **373**, 1697–1708 (2015).
13. C. H. Marshall *et al*., Differential response to olaparib treatment among men with metastatic castration-resistant prostate cancer harboring BRCA1 or BRCA2 versus ATM mutations. *Eur. Urol.* 10.1016/j.eururo.2019.02.002 (2019).
14. J. C. Amé *et al*., PARP-2, A novel mammalian DNA damage-dependent poly(ADP-ribose) polymerase. *J. Biol. Chem.* **274**, 17860–17868 (1999).
15. V. Schreiber *et al*., Poly(ADP-ribose) polymerase-2 (PARP-2) is required for efficient base excision DNA repair in association with PARP-1 and XRCC1. *J. Biol. Chem.* **277**, 23028–23036 (2002).
16. P. Bai *et al*., Poly(ADP-ribose) polymerase-2 [corrected] controls adipocyte differentiation and adipose tissue function through the regulation of the activity of the retinoid X receptor/peroxisome proliferator-activated receptor-gamma [corrected] heterodimer. *J. Biol. Chem.* **282**, 37738–37746 (2007).
17. F. Dantzer *et al*., Poly(ADP-ribose) polymerase-2 contributes to the fidelity of male meiosis I and spermiogenesis. *Proc. Natl. Acad. Sci. U.S.A.* **103**, 14854–14859 (2006).
18. J. Yélamos *et al*., PARP-2 deficiency affects the survival of CD4+CD8+ double-positive thymocytes. *EMBO J.* **25**, 4350–4360 (2006).
19. A. Saxena *et al*., Poly(ADP-ribose) polymerase 2 localizes to mammalian active centromeres and interacts with PARP-1, Cenpa, Cenpb and Bub3, but not Cenpc. *Hum. Mol. Genet.* **11**, 2319–2329 (2002).
20. F. Dantzer *et al*., Functional interaction between poly(ADP-ribose) polymerase 2 (PARP-2) and TRF2: PARP activity negatively regulates TRF2. *Mol. Cell. Biol.* **24**, 1595–1607 (2004).
21. J. Yélamos, V. Schreiber, F. Dantzer, Toward specific functions of poly(ADP-ribose) polymerase-2. *Trends Mol. Med.* **14**, 169–178 (2008).
22. P. Bai *et al*., PARP-2 regulates SIRT1 expression and whole-body energy expenditure. *Cell Metab.* **13**, 450–460 (2011).
23. M. Szántó *et al*., Poly(ADP-ribose) polymerase-2: Emerging transcriptional roles of a DNA-repair protein. *Cell. Mol. Life Sci.* **69**, 4079–4092 (2012).
24. J. C. Brenner *et al*., Mechanistic rationale for inhibition of poly(ADP-ribose) polymerase in ETS gene fusion-positive prostate cancer. *Cancer Cell* **19**, 664–678 (2011).
25. M. J. Schiewer *et al*., Dual roles of PARP-1 promote cancer growth and progression. *Cancer Discov.* **2**, 1134–1149 (2012).
26. E. Kounatidou *et al*., A novel CRISPR-engineered prostate cancer cell line defines the AR-V transcriptome and identifies PARP inhibitor sensitivities. *Nucleic Acids Res.*, gkz286 (2019).
27. D. C. Koboldt *et al*., Rare variation in TET2 is associated with clinically relevant prostate carcinoma in African Americans. *Cancer Epidemiol. Biomarkers Prev.* **25**, 1456–1463 (2016).
28. Cancer Genome Atlas Research Network, The molecular taxonomy of primary prostate cancer. *Cell* **163**, 1011–1025 (2015).
29. J. H. Luo *et al*., Gene expression analysis of prostate cancers. *Mol. Carcinog.* **33**, 25–35 (2002).
30. C. J. Best *et al*., Molecular alterations in primary prostate cancer after androgen ablation therapy. *Clin. Cancer Res.* **11**, 6823–6834 (2005).
31. B. S. Taylor *et al*., Integrative genomic profiling of human prostate cancer. *Cancer Cell* **18**, 11–22 (2010).
32. A. Liberzon *et al*., The Molecular Signatures Database (MSigDB) hallmark gene set collection. *Cell Syst.* **1**, 417–425 (2015).
33. A. Subramanian *et al*., Gene set enrichment analysis: A knowledge-based approach for interpreting genome-wide expression profiles. *Proc. Natl. Acad. Sci. U.S.A.* **102**, 15545–15550 (2005).
34. R. Pellicciari *et al*., On the way to selective PARP-2 inhibitors. Design, synthesis, and preliminary evaluation of a series of isoquinolinone derivatives. *ChemMedChem* **3**, 914–923 (2008).
35. F. Moroni *et al*., Selective PARP-2 inhibitors increase apoptosis in hippocampal slices but protect cortical cells in models of post-ischaemic brain damage. *Br. J. Pharmacol.* **157**, 854–862 (2009).
36. J. Lovén *et al*., Selective inhibition of tumor oncogenes by disruption of super-enhancers. *Cell* **153**, 320–334 (2013).
37. M. M. Pomerantz *et al*., The androgen receptor cistrome is extensively reprogrammed in human prostate tumorigenesis. *Nat. Genet.* **47**, 1346–1351 (2015).
38. J. Murai *et al*., Trapping of PARP1 and PARP2 by clinical PARP inhibitors. *Cancer Res.* **72**, 5588–5599 (2012).
39. G. D'Alessandro, F. d'Adda di Fagagna, Transcription and DNA damage: Holding hands or crossing swords? *J. Mol. Biol.* **429**, 3215–3229 (2017).
40. M. C. Haffner *et al*., Androgen-induced TOP2B-mediated double-strand breaks and prostate cancer gene rearrangements. *Nat. Genet.* **42**, 668–675 (2010).
41. W. R. Polkinghorn *et al*., Androgen receptor signaling regulates DNA repair in prostate cancers. *Cancer Discov.* **3**, 1245–1253 (2013).
42. S. Stelloo *et al*., Endogenous androgen receptor proteomic profiling reveals genomic subcomplex involved in prostate tumorigenesis. *Oncogene* **37**, 313–322 (2018).
43. Y. Zhang *et al*., Nucleation of DNA repair factors by FOXA1 links DNA demethylation to transcriptional pioneering. *Nat. Genet.* **48**, 1003–1013 (2016).
44. Y. C. Liang, C. Y. Hsu, Y. L. Yao, W. M. Yang, PARP-2 regulates cell cycle-related genes through histone deacetylation and methylation independently of poly(ADP-ribosyl) ation. *Biochem. Biophys. Res. Commun.* **431**, 58–64 (2013).
45. Z. Liu, W. L. Kraus, Catalytic-independent functions of PARP-1 determine Sox2 pioneer activity at intractable genomic loci. *Mol. Cell* **65**, 589–603 e9 (2017).
46. C. E. Knezevic *et al*., Proteome-wide profiling of clinical PARP inhibitors reveals compound-specific secondary targets. *Cell Chem. Biol.* **23**, 1490–1503 (2016).
47. P. Jelinic, D. A. Levine, New insights into PARP inhibitors' effect on cell cycle and homology-directed DNA damage repair. *Mol. Cancer Ther.* **13**, 1645–1654 (2014).
48. H. Pu *et al*., PARP-1 regulates epithelial-mesenchymal transition (EMT) in prostate tumorigenesis. *Carcinogenesis* **35**, 2592–2601 (2014).
49. D. Zheng *et al*., Secretory leukocyte protease inhibitor is a survival and proliferation factor for castration-resistant prostate cancer. *Oncogene* **35**, 4807–4815 (2016).

SI Appendix, Supplementary Materials and Methods

Western blot and RT-qPCR

Western blot and RT-qPCR were performed as previously described (1). Antibodies and primer sequences used are listed in SI Appendix, Table S1.

Plasmid and siRNA transfection

FLAG-tagged PARP-1 and PARP-2 mammalian expression plasmids were obtained from Dr. Guy G. Poirier (Université Laval, Québec) (2). pEGFP-PARP2 wild-type and E545A mutant plasmids were obtained from Dr. Xiaochun Yu (City of Hope Medical Center, Duarte, CA) (3). pCDNA3.1-Flag-FOXA1 was obtained from Dr. Yongfeng Shang (Peking University, Beijing, China) (4). pGL3-PSA540-enhancer (PSA-luc) and ARR3-tk-luc (Probasin-luc) reporter plasmids were described previously (5). The pRL-CMV Renilla luciferase reporter was purchased from Promega. Plasmid transfection was performed using X-tremeGENE HP DNA transfection reagent (Sigma-Aldrich) according to the manufacturer's instructions. siRNAs were purchased from Sigma-Aldrich (SI Appendix, Table S1). Reverse transfection with siRNAs (20 nM) was performed using Lipofectamine RNAiMAX transfection reagent (Life Technologies) according to the manufacturer's instructions.

CRISPR/Cas9 gene knockout

CRISPR guides targeting PARP-1 or PARP-2 were cloned into lentiGuide-Puro vector (#52963; Addgene). The single guide RNA (sgRNA) vector targeting GFP was obtained from Dr. William C. Hahn (DFCI) as a gift. The lentiCas9-Blast vector that expresses Cas9 was obtained from Addgene (#52962). To generate the PARP KO cell lines, LNCaP cells were co-infected with lentiviruses carrying Cas9 and sgRNA as indicated, and selected with Puromycin (2 μg/ml) and Blasticidin (10 μg/ml) for two weeks. The sgRNA sequences are listed in the SI Appendix, Table

S1. In addition, we generated a PARP-2 KO LNCaP cell line and a non-target (NT) control line using RNP delivery. Cells were con-transfected with purified Cas9 nuclease protein (#CAS11200; Dharmacon) in conjunction with synthetic PARP-2 sgRNA (50nM) or NT sgRNA (50nM) using DharmaFECT Duo Transfection Reagent (#T-2010-01; Dharmacon) according to the manufacturer's instructions. Synthetic sgRNA is made by mixing equal amounts of Edit-R synthetic PARP-2 crRNA (#CM-010127-01-0002; Dharmacon) or NT control crRNA (#U-007501-01-05; Dharmacon) with Edit-R synthetic tracrRNA (#U-002005-20; Dharmacon).

Cell viability

Prostate cancer (PCa) cells were seeded in 96-well plates ($5x10^3$-$2x10^4$ cells/well) and treated as indicated. Cells were maintained in culture media for seven days before viability measurement using the alamarBlue assay kit (Thermo Fisher Scientific).

Soft agar and colony formation assay

For soft agar assays, PARP KD/KO cells ($5x10^3$ cell/well) were suspended in media with 0.6% Noble agar and seeded on the top of the bottom gel with media containing 1% Noble agar in 6-well plates. Cells were maintained in culture media for three weeks. Colonies were stained by nitroblue tetrazolium chloride solution. Colony formation assays were performed by seeding PARP KD ($5x10^3$ cells/well) or KO cells ($1x10^3$ cells/well) into 6-well plates. Cells were maintained in culture media for 14 days. The colonies were stained with crystal violet.

Xenograft tumor assay

For LNCaP PARP-1 and PARP-2 KO models, cells ($1x10^6$ cells/site) were subcutaneously injected into 8-week-old male ICR-SCID mice (Taconic Laboratories). The tumor growth was measured weekly using a vernier caliper, and the tumor volume was calculated according to the formula: volume = length×width^2/2. For the VCaP model, cells ($2x10^6$/site) were subcutaneously

injected into 8-week-old male ICR-SCID mice. Mice bearing about 150 mm^3 tumors were randomized into three treatment groups and treated with UPF-1069 (50 mg/kg), olaparib (50 mg/kg), or DMSO (5%) in 30% PEG300 daily by intraperitoneal injection for 3.5 weeks. Tumors were measured weekly using the method described above.

PARP activity assay

In vitro PARP activity assays were performed using PARP Universal Colorimetric Assay Kit (#4677-096-K; Trevigen) according to the manufacturer's instructions. Briefly, whole cell lysates were extracted using 1×PARP buffer containing 0.4 M NaCl, 1% Triton X-100, and proteases inhibitors. A total of 5 μg protein was loaded into the plates and followed by incubation for 1 hour. Plates were read in a spectrophotometer at 450 nm. Relative PARP activity was calculated based on the standard curve generated using the PARP-HSA enzyme provided in the kit. To assess the selectivity of PARP inhibitors (PARPi), LNCaP cells were transfected with FLAG-tagged PARP-1, PARP-2, or vector for 48 hours before treatment with PARPi (10 μM) for additional 4 hours. Whole cell lysates were extracted using RIPA buffer with protease, phosphatase and PARG inhibitors. The *in vivo* PARP activity was determined by Western blot using the antibody against poly(ADP-ribose).

Biotinylated small molecule pull-down assay

The process of Biotin-UPF-1069 and Biotin-olaparib synthesis is described in SI Appendix, Fig. S4. Biotinylated small molecules (500 μM) were immobilized on Dynabeads MyOne Streptavidin T1 beads (Invitrogen) in lysis buffer (50 mM Tris-HCl, pH-8.0; 5% glycerol, 1.5 mM $MgCl_2$, 100 mM NaCl, 0.2% NP-40, 1 mM DTT, 1 x protease inhibitor, and phosphatase inhibitor). D-Biotin (#00033; Chem Impex Int'L Inc) was used as a negative control. Cell lysates were extracted from LNCaP cells with lysis buffer and pre-incubated with unmodified UPF-1069, olaparib (20 μM) or DMSO for 30 minutes at 4°C. Affinity pull-down experiments were performed by incubating lysates

with Biotin-UPF-1069 or Biotin-olaparib coated beads for 2 hours at 4 °C. After washing with lysis buffer, bound proteins were eluted by boiling in 2 x SDS protein loading buffer and detected by Western blot.

Co-immunoprecipitation (co-IP)

To examine endogenous PARP-2 and FOXA1 interaction, nuclear proteins were extracted from LNCaP cells using the Subcellular Protein Fractionation Kit (Thermo Fisher Scientific), diluted with 1.5 volume of Co-IP buffer (50 mM Tris-HCl, pH 8.0, 120 mM NaCl, 0.3% NP40, 1 mM EDTA, 1 x protease inhibitor, phosphatase inhibitors, and PARG inhibitor), and incubated with a specific antibody (1 µg) for 18 hours at 4 ºC with constant rotation. Protein A/G magnetic beads (Thermo Fisher Scientific) were added for another 2 hours incubation before being washed five times with Co-IP buffer. Immunoprecipitated proteins were eluted with 2 x SDS protein loading buffer and analyzed by Western blot. For PARPi treatment experiments, LNCaP cells were pre-treated with PARPi (10 µM) for 6 hours. Nuclear proteins were extracted with PARPi (0.5 µM) added into the fractionation and Co-IP buffers.

GST Pull-down

Purified GST-PARP2 protein (#PAR-21-347) was purchased from Reaction Biology Corporation. Flag-FOXA1 protein was synthesized using TNT T7 Quick Coupled Transcription/Translation System (L1170; Promega) with 1 µg pCDNA3.1-Flag-FOXA1 plasmid according to the manufacturer's instruction. The TNT product Flag-FOXA1 protein was pre-incubated in 1 x PBS buffer supplied with 0.8% BSA and 1 x protease inhibitor at 4°C for 30 min. At the same time, the GST-PARP2 protein was incubated with glutathione magnetic agarose beads (#78601; Thermo Scientific) at 4°C for 30 min. The beads carrying GST-PARP2 protein and Flag-FOXA1 protein solution were mixed and incubated at 4°C overnight. The beads were washed with washing buffer (0.5% NP-40 in 1 x PBS) 5 times and eluted with 2 x SDS protein loading buffer for western

blotting. The equal molar of tag-free GST protein (SRP5348; Sigma) was used as negative control.

Chromatin immunoprecipitation (ChIP)

ChIP experiments were performed as previously described (6). Briefly, LNCaP cells were grown in the regular media with 10% fetal bovine serum (FBS) without dihydrotestosterone (DHT) stimulation. The cells were treated with DMSO or PARPi (10 μM) for 16 hours before being cross-linked. For the ChIP experiments with gene KD, LNCaP cells were transfected with PARP-1, PARP-2, or non-specific control (NC) siRNA (20 nM) for 3 days before being harvested. Chromatin was fragmented by sonication and immunoprecipitated by 2 μg antibodies as indicated. ChIP DNA was then extracted and analyzed by TaqMan qPCR using iTaq Universal Probes Supermix (Bio-Rad). The primer and probe sequences are listed in SI Appendix, Table S1.

ChIP-sequencing (ChIP-seq)

ChIP experiments with two biological replicates for each treatment were performed. Purified ChIP DNA was dissolved in TE buffer and re-sheared using Covaris sonicator to enable enrichment of fragments with an average size of 300 bp. The re-sheared DNA samples were purified for library preparation using the minElute PCR purification kit (Qiagen). The ChIP-seq libraries were prepared using the ThruPLEX DNA-seq Kit (R400427; Rubicon Genomics). The libraries were sequenced in the NextSeq500 System (Illumina). ChIP-seq data was mapped to human genome (hg19) using Bowtie2 (v2.3.0) (7) with default settings. Reads that did not map uniquely were removed. To assess the biological variability of the ChIP-seq experiments, deepTools2 program (v2.4.0) (8) was employed to perform an unsupervised hierarchical clustering analysis using normalized enrichment levels, and to calculate the Pearson correlation scores between each sample (SI Appendix, Fig. S13). To compare the genome-wide distribution, MACS2 (2.1.1) (9) was used to identify AR ($q < 0.05$), FOXA1 ($q < 0.01$), and H3K27Ac (broad peak calling mode,

cut-off 0.1) binding sites with default parameters and input sample as a control. Motif analysis was performed using Homer (v4.9) (10) with default settings. The deepTools2 was used to calculate the genomic coverage of each factor, and to generate the heatmap and enrichment plots. Genome-wide binding sites of AR and FOXA1 were centered by its peak summit and ranked by the average coverage within 2.5 kb relative to the peak center. The coverage for other samples within ranked binding sites was plotted accordingly. The UCSC genome browser (11) was employed to visualize the ChIP-seq binding signals. ChIP-seq data have been deposited into the Gene Expression Omnibus (GEO) database (GSE114275).

RNA-sequencing (RNA-seq)

Total RNA was extracted from cells using the RNeasy Mini Kit (Qiagen). RNA-seq libraries were prepared using NEBNext Ultra RNA Library Prep Kit (E7530; New England BioLabs), followed by next generation sequencing using the NextSeq500 System (Illumina). RNA-seq data was mapped to human genome (hg19) using Tophat2 (v2.1.0) (12). Raw counts were generated using HTseq (v0.6.1) (13) and the union method with default parameters. Genes that had at least 1 read per million in at least half of the samples were kept for further analysis. Differentially expressed genes ($p < 0.01$, FDR < 0.01, and fold of change > 1.75) were identified using the EdgeR package (3.12.0) (14) for R.

To calculate the overlap between the differentially expressed gene lists and the “Hallmarks” and “KEGG” gene expression signatures in the MSigDB database, GSEA annotation tools (http://software.broadinstitute.org/gsea/msigdb/annotate.jsp) were employed with a *q*-value below 0.05. GSEA was carried out using the GSEA software package (15) to assess the enrichment of “hallmark androgen response” gene signature. The normalized enrichment scores (NES) and adjusted *p*-values were computed using the GSEA method based on 1,000 random permutations of the ranked genes. The RNA-seq data have been deposited into the Gene Expression Omnibus (GEO) database (GSE114275).

Clinical dataset analysis

To study the association between the expression levels of PARPs and the aggressiveness of PCa, RNA-seq V2 RSEM gene expression data (Z-scores) and follow-up data were obtained from TCGA (Provisional) through cBioPortal (16). Unsupervised hierarchical clustering and the Pearson correlation between expression levels and Gleason scores were calculated using R. In addition, patients were split into two groups with high (> medium) or low (≤ medium) expression of PARP-1, PARP-2, and PARP-11, respectively. The Kaplan-Meier plots of biochemical recurrence-free survival proportion of each group were generated by GraphPad. Statistical analyses were performed using log-rank (Mantel-Cox) test. Gene expression levels of PARP-1, PARP-2, and PARP-11 from other datasets were obtained from GEO, Oncomine or cBioPortal (17-19). Statistical analyses were performed using a two-tailed Student's *t*-test.

Tissue microarrays (TMAs) and Immunohistochemistry (IHC) analysis

The TMAs were constructed and IHC was performed as previously described (20, 21). Prostate tumor samples were retrieved from the Vancouver Prostate Centre Tissue Bank, comprised of 232 benign prostate, 819 primary PCa, and 78 CRPC cores. The CRPC tumors were from patients who had received hormonal therapies and been diagnosed with CRPC. IHC was performed by Ventana Discovery XT autostainer with PARP-2 antibody (#39743; Active Motif). The IHC images were evaluated and scored by pathologist Dr. Ladan Fazli.

References

1. Zheng D*, et al.* (2016) Secretory leukocyte protease inhibitor is a survival and proliferation factor for castration-resistant prostate cancer. *Oncogene* 35(36):4807-4815.
2. Rouleau M*, et al.* (2007) PARP-3 associates with polycomb group bodies and with components of the DNA damage repair machinery. *Journal of cellular biochemistry* 100(2):385-401.
3. Chen Q, Kassab MA, Dantzer F, & Yu X (2018) PARP2 mediates branched poly ADP-ribosylation in response to DNA damage. *Nat Commun* 9(1):3233.
4. Zhang Y*, et al.* (2016) Nucleation of DNA repair factors by FOXA1 links DNA demethylation to transcriptional pioneering. *Nat Genet* 48(9):1003-1013.
5. Jia L*, et al.* (2003) Androgen receptor activity at the prostate specific antigen locus: steroidal and non-steroidal mechanisms. *Mol Cancer Res* 1(5):385-392.
6. Decker KF*, et al.* (2012) Persistent androgen receptor-mediated transcription in castration-resistant prostate cancer under androgen-deprived conditions. *Nucleic acids research* 40(21):10765-10779.
7. Langmead B & Salzberg SL (2012) Fast gapped-read alignment with Bowtie 2. *Nat Methods* 9(4):357-359.
8. Ramirez F*, et al.* (2016) deepTools2: a next generation web server for deep-sequencing data analysis. *Nucleic acids research* 44(W1):W160-165.
9. Zhang Y*, et al.* (2008) Model-based analysis of ChIP-Seq (MACS). *Genome Biol* 9(9):R137.
10. Heinz S*, et al.* (2010) Simple combinations of lineage-determining transcription factors prime cis-regulatory elements required for macrophage and B cell identities. *Molecular cell* 38(4):576-589.
11. Kent WJ*, et al.* (2002) The human genome browser at UCSC. *Genome Res* 12(6):996-1006.
12. Trapnell C, Pachter L, & Salzberg SL (2009) TopHat: discovering splice junctions with RNA-Seq. *Bioinformatics* 25(9):1105-1111.
13. Anders S, Pyl PT, & Huber W (2015) HTSeq--a Python framework to work with high-throughput sequencing data. *Bioinformatics* 31(2):166-169.
14. Robinson MD, McCarthy DJ, & Smyth GK (2010) edgeR: a Bioconductor package for differential expression analysis of digital gene expression data. *Bioinformatics* 26(1):139-140.
15. Subramanian A*, et al.* (2005) Gene set enrichment analysis: a knowledge-based approach for interpreting genome-wide expression profiles. *Proceedings of the National Academy of Sciences of the United States of America* 102(43):15545-15550.
16. Cancer Genome Atlas Research N (2015) The Molecular Taxonomy of Primary Prostate Cancer. *Cell* 163(4):1011-1025.
17. Luo JH*, et al.* (2002) Gene expression analysis of prostate cancers. *Molecular carcinogenesis* 33(1):25-35.
18. Best CJ*, et al.* (2005) Molecular alterations in primary prostate cancer after androgen ablation therapy. *Clin Cancer Res* 11(19 Pt 1):6823-6834.
19. Taylor BS*, et al.* (2010) Integrative genomic profiling of human prostate cancer. *Cancer cell* 18(1):11-22.
20. Xie N*, et al.* (2015) The expression of glucocorticoid receptor is negatively regulated by active androgen receptor signaling in prostate tumors. *Int J Cancer* 136(4):E27-38.
21. Li H*, et al.* (2016) UGT2B17 Expedites Progression of Castration-Resistant Prostate Cancers by Promoting Ligand-Independent AR Signaling. *Cancer Res* 76(22):6701-6711.

SI Appendix, Fig. S1

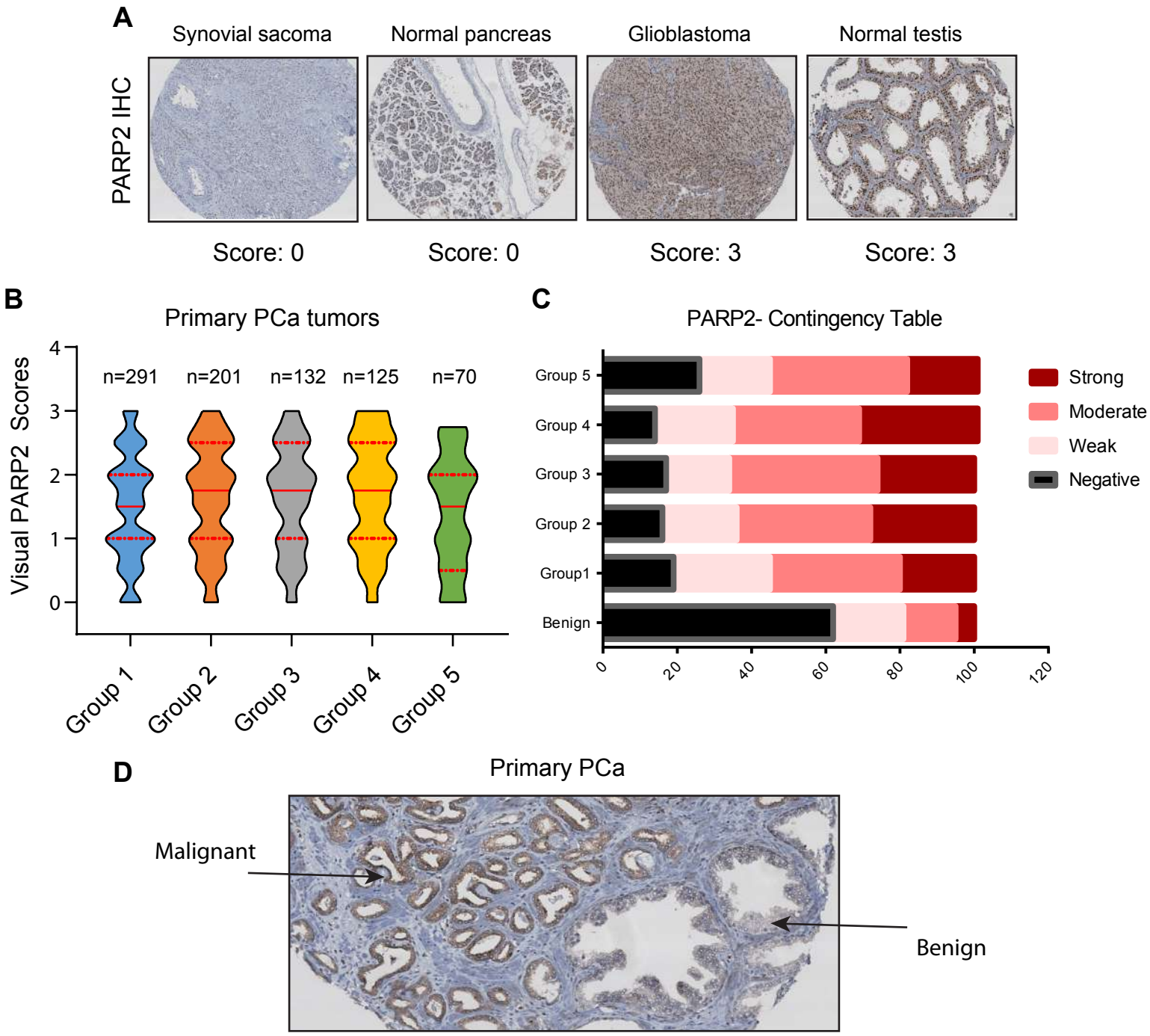

Fig. S1. Tissue microarray (TMA) and immunohistochemistry (IHC) analyses. **(A)** Three PARP-2 antibodies (anti-PARP-2, clone 4G8, MABE18, Sigma-Aldrich; anti-PARP-2, HPA052003, Sigma-Aldrich; anti-PARP-2, #39743, Active Motif) were tested on a multiorgan TMA with 156 tissue cores. The anti-PARP-2 from Active Motif was chosen for this study. IHC signal intensity was scored as 0, 1, 2, 3 corresponding to negative, weak, moderate, and strong PARP-2 protein expression. Four representative IHC images (magnification 10x) are presented, including normal pancreas (negative) and nomal testis (strong), which are consistent with the mRNA expression levels from the databae - GTExPortal (www.gtexportal.org). **(B)** The primary prostate cancer (PCa) tumors were assigned into 5 Grade Groups: Group 1 (Gleason score ≤6), Group 2 (Gleason score 3+4=7), Group 3 (Gleason score 4+3=7), Group 4 (Gleason score 8), and Group 5 (Gleason score 9-10). The expression levels of PARP-2 were quantified by visual scoring and shown in a violin plot. Red solid lines represent the median, and dashed lines are the 25th and 75th percentile. No statistical significance was reached by Kruskal-Wallis test. **(C)** The PARP-2 contingency table shows the percentage of tissue cores in each score group sorted by Gleason score. **(D)** The image (magnification 20x) shows differential PARP-2 expression in malignant cells (high expression) vs. benign cells (low expression) in the same tissue core.

SI Appendix, Figure S2

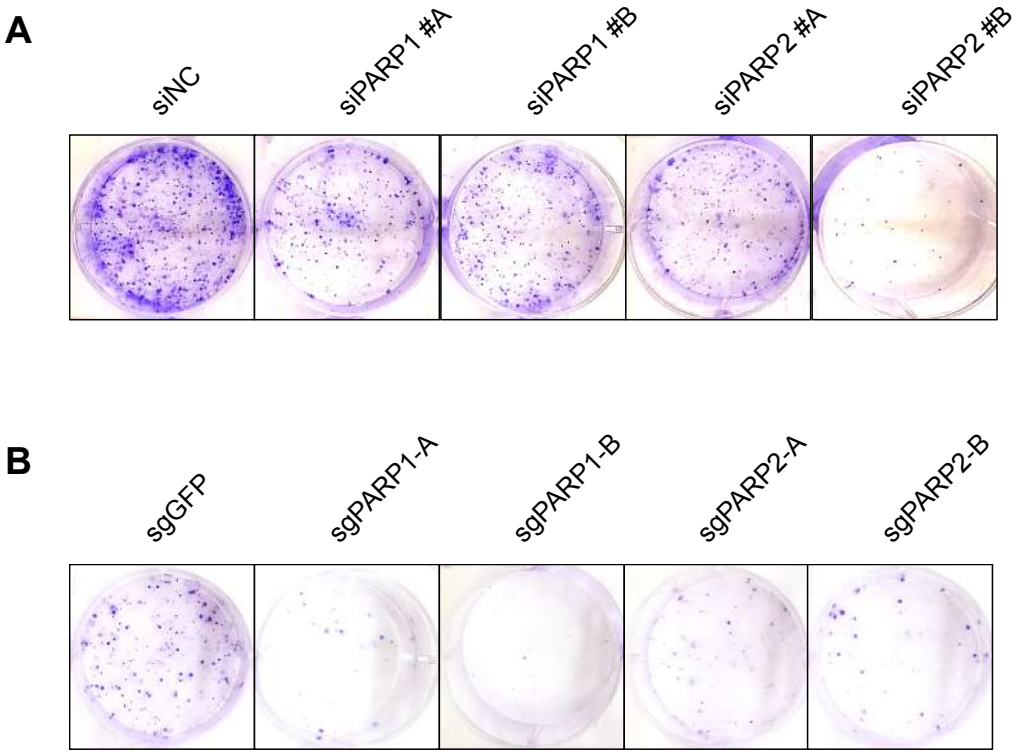

Fig. S2. Inhibition of PARP-2 attenuates clonogenic growth of LNCaP cells. The images show colony formation of LNCaP cells after knockdown **(A)** or knockout **(B)** of PARP-1 and PARP-2. All experiments were repeated at least three times.

SI Appendix, Fig. S3

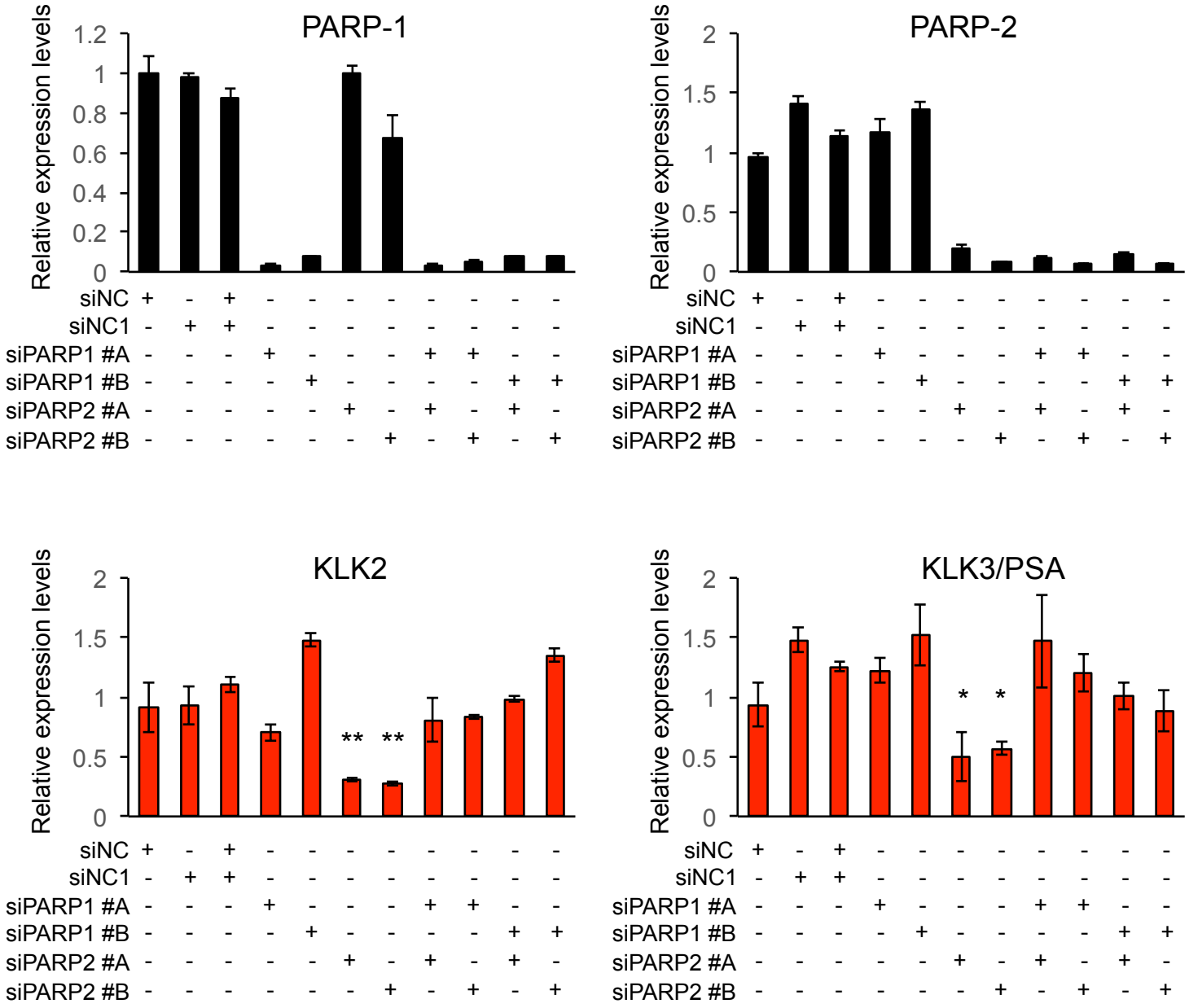

Fig. S3. Knockdown (KD) of PARP-2 alone inhibits the expression of KLK2 and KLK3/PSA. LNCaP cells were transfected with PARP-1 and/or PARP-2 siRNA (20 nM) as indicated. Two non-specific control (NC) siRNAs were used. The mRNA levels of PARP-1, PARP-2, KLK2, and KLK3/PSA were examined by RT-qPCR two days after siRNA KD. All data represent the mean ± SD from three PCR replicates. Statistical significance betwen siPARP1/siPARP2 vs. siNS/siNS1 was determined by a two-tailed Student's *t*-test. *. $p<0.05$; **, $p<0.01$.

SI Appendix, Fig. S4

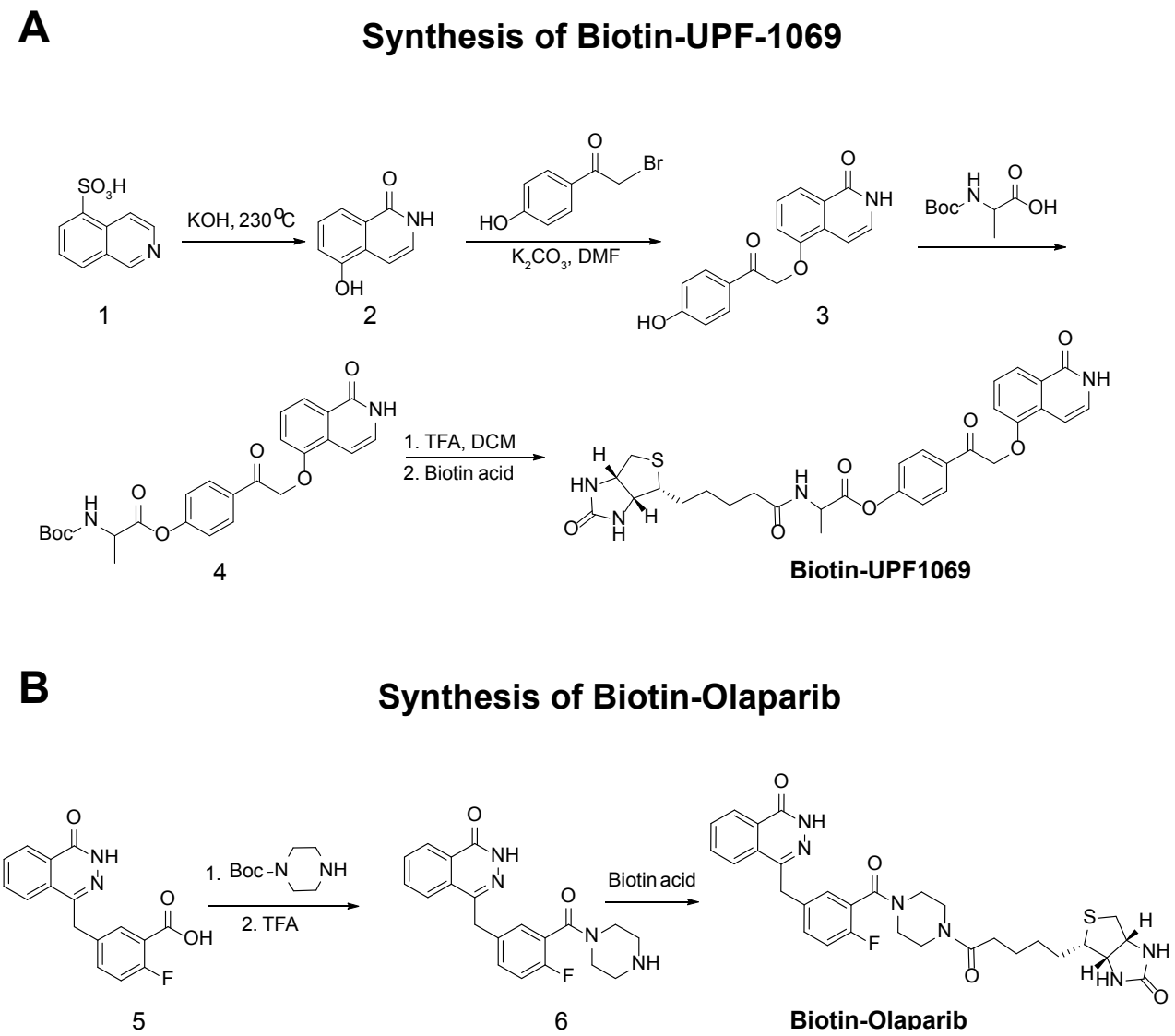

Fig. S4. Synthesis of Biotinylated PARP inhibitors. **(A)** Scheme of the synthetic route for Biotin-UPF1069. Briefly, 5-Isoquinoline sulfonic acid 1 was fused with KOH for compound 2 and then reacted with 2-bromo-4'-hydroxyacetophenone to give 3. Compound 3 was coupled with (t-butoxycarbonyl)alanine for 4, followed by de-Boc with TFA and amide coupling with biotin acid to give Biotin-UPF-1069. **(B)** Scheme of the synthetic route for Biotin-olaparib. Commercially available compound 5 was coupled with t-butyl piperazine-1-carboxylate for 6 then followed by the treated with TFA for de-Boc to yield Biotin-Olaparib. The structure of all the products was confirmed by LC-MS analysis.

SI Appendix, Fig. S5

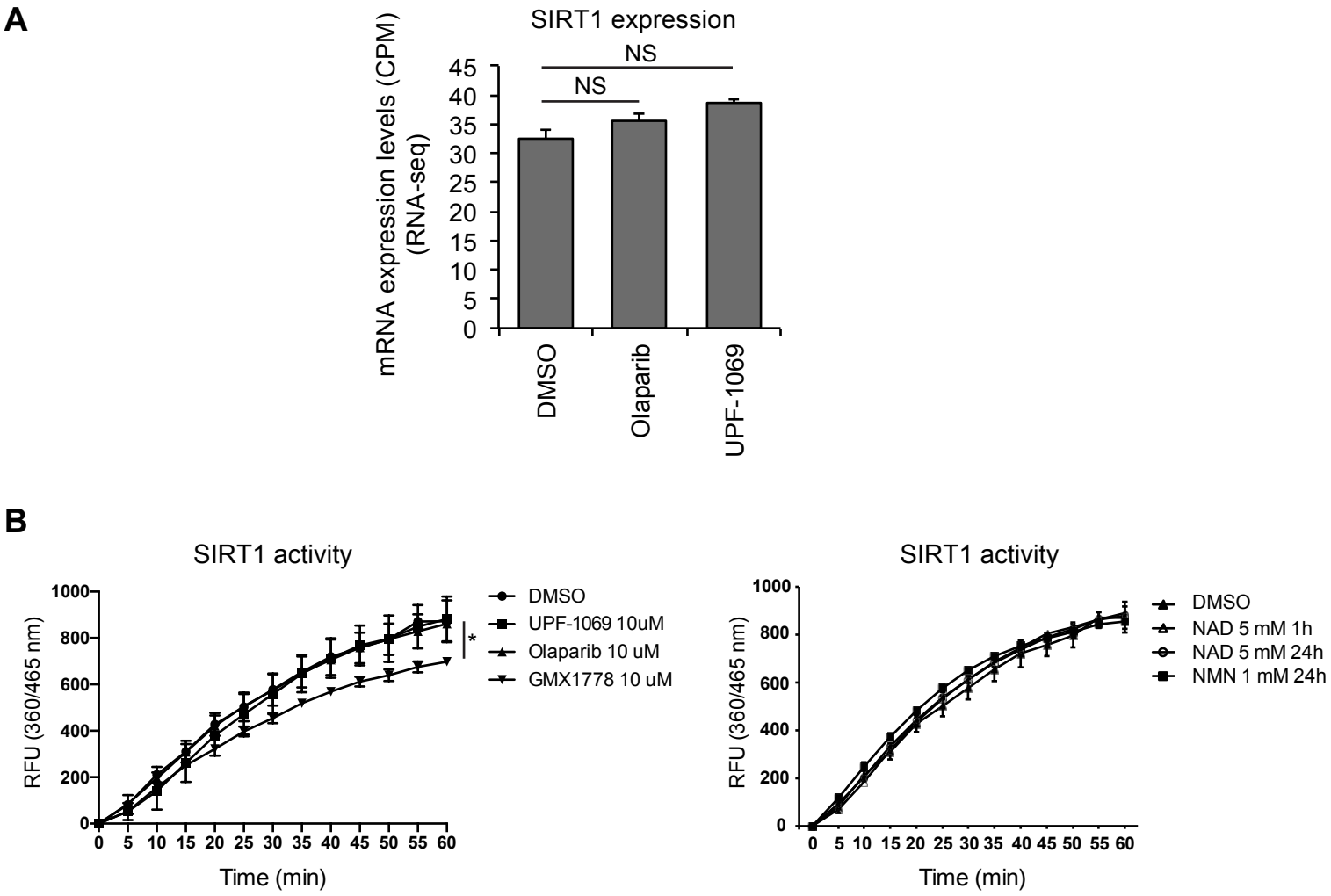

Fig. S5. SIRT1 expression and activity remain unchanged after treatment with PARP inhibitors. **(A)** RNA-seq results show the treatment with olaparib or UPF-1069 has no significant (NS) effect on SIRT1 mRNA expression in LNCaP cells. **(B)** The treatment with olaparib or UPF-1069 does not affect SIRT1 activity. In contrast, the NAMPT inhibitor, GMX1778, which blocks NAD+ biosynthesis, significantly decreases SIRT1 activity. The addition of NAD (Sigma-Aldrich, N3014) or NAD precursor, NMN (Sigma-Aldrich, N3501) has no effect on SIRT1 activity. All data represent the mean ± SD. Statistical significance was determined by a two-tailed Student's *t*-test. *. $p<0.05$. RFU = relative fluorescence unit.

SIRT1 activity assay: The deacetylase activity of SIRT1 was determined using a SIRT1 Activity Assay Kit (ab156065; Abcam) according to the manufacturer's instruction with modification. Briefly, LNCaP cells (2 x 10e5 cells/well) were seeded in a 6-well plate well. Cells were treated with UPF-1069 (10 μM), Olaparib (10 μM) or GMX1778 (10 μM) for 24 hours. In a separate experiment, NAD (5 mM) or NMN (1 mM) was added into cell culture for 1 hour or 24 hours. Whole cell lysates were extracted using RIPA buffer (10 mM Tris/Cl pH 7.5; 150 mM NaCl; 0.5 mM EDTA; 0.1% SDS; 1% TRITON X-100; 1% Deoxycholate) supplied with 1x protein Inhibitor cocktail (Sigma). Cell lysates (100 μg) were incubated with Fluoro-Substrate Peptide Solution and SIRT1 Assay Buffer. Fluorescence intensity was then measured over time as indicated using a microplate reader with excitation at 356 nm and emission at 460 nm.

SI Appendix, Fig. S6

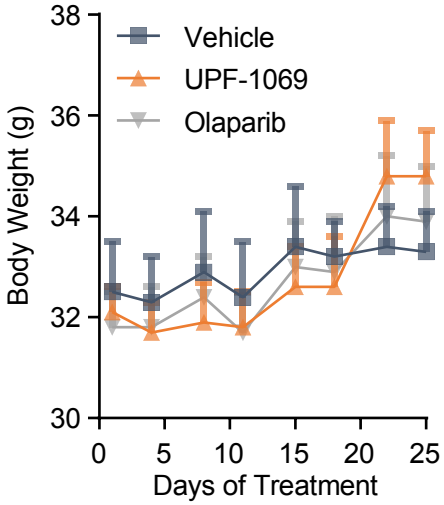

Fig. S6. Effect of PARP inhibitors on the body weight of tumor-bearing mice. The total body weight of tumor-bearing mice (n=7 for each group) after treatment of UPF-1069, olaparib, or vehicle was measured. Data represent the Mean ± SD.

Appendix, Fig. S7

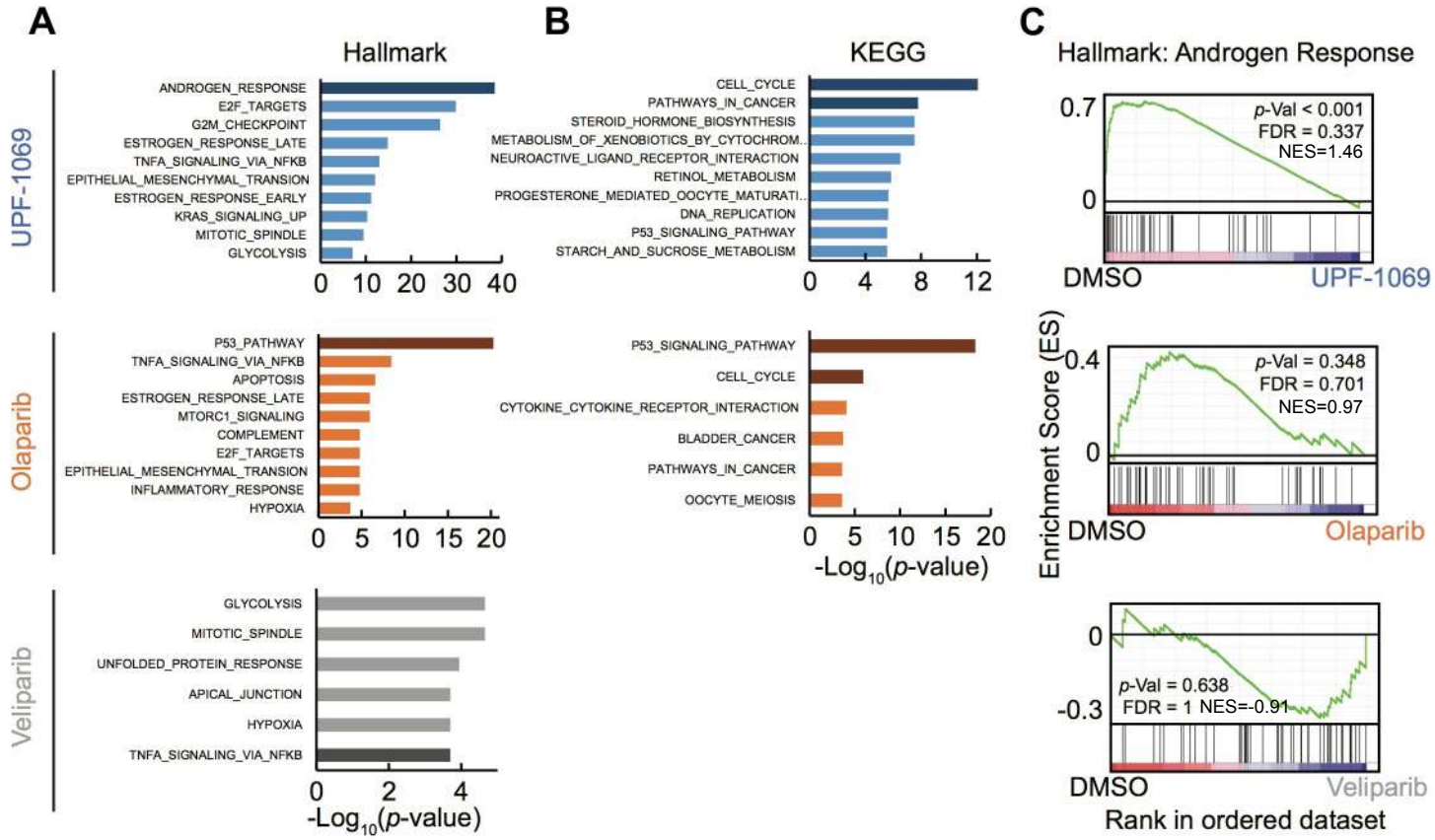

Fig. S7. UPF-1069 treatment alters androgen receptor (AR) target gene expresion. **(A)** Enrichment of Hallmark signatures in UPF-1069-, olaparib-, and veliparib-altered genes. **(B)** Enrichment of KEGG signatures in UPF-1069-, olaparib-, and veliparib-altered genes. **(C)** GSEA was used to test for enrichment of the “androgen response” gene signature in UPF-1069-, olaparib-, or veliparib-altered genes. The GSEA reveals significant repression of “androgen response” genes after treatment with UPF-1069 (p<0.001; FDR=0.337; NES=1.46) but not with olaparib (p=0.348; FDR=0.701; NES=0.97) or veliparib (p=0.638; FDR=1; NES=-0.91). Analyses were described in the Materials and Methods. FDR = false discovery rate; NES = normalized enrichment score.

SI Appendix, Fig. S8

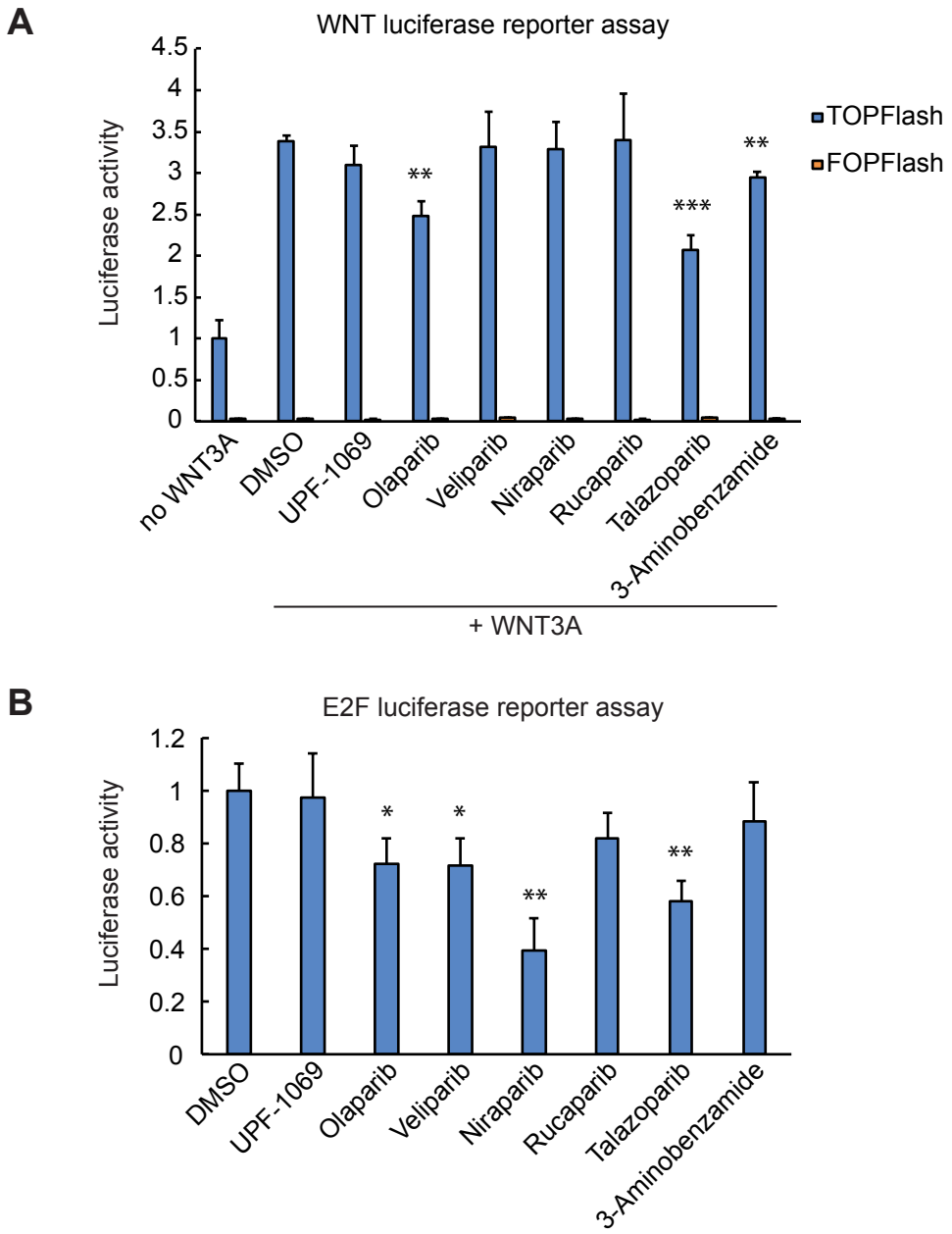

Fig. S8. Inhibitory effects of PARP inhibitors (PARPi) on WNT and E2F signaling. **(A)** HCT116 colon cancer cells were transfected with TOPFlash or FOPFlash luciferase reporter plasmids as previously described (1). Cells were stimulated with WNT3A (50 ng/ml) and treated with PARPi (10 μM) as indicated for 24 hours. Luciferase activity was measured using Dual-Glo Luciferase Assay System (E2920; Promega). The luciferase activity was normalized to co-transfected pRL-CMV Renilla luciferase control reporter activity. **(B)** LNCaP cells were transfected with E2F luciferase reporter and treated with PARPi (10 μM) as indicated for 24 hours. Luciferase activity was measured as described in **(A)**. E2F luciferase reporter plasmid was obtained from Dr. Joshua B. Rubin (Washington University in St. Louis) as a gift. The reporter construct contains three tandem E2F consensus elements subcloned into SacI/XhoI sites of the pGL4.26 vector (Promega) upstream of a minimal promoter. E2F consensus sequence (TGCAATTTCGCGCCAAACTTG) was previously described (2). Each PARPi was compared to the DMSO control. All data represent the mean ± SD from three replicates. Statistical significance was determined by a two-tailed Student's *t*-test. *, $p < 0.05$; **, $p < 0.01$; ***, $p<0.001$.

References:

1. Zheng D, Decker KF, Zhou T, Chen J, Qi Z, Jacobs K, Weilbaecher KN, Corey E, Long F, Jia L. Role of WNT7B-induced noncanonical pathway in advanced prostate cancer. Mol Cancer Res 2013; 11(5):482-93.

2. Hiebert SW, Blake M, Azizkhan J, Nevins JR. Role of E2F transcription factor in E1A-mediated transactivation of cellular genes. J Bio Chem 1991; 65(7):3547-52.

SI Appendix, Fig. S9

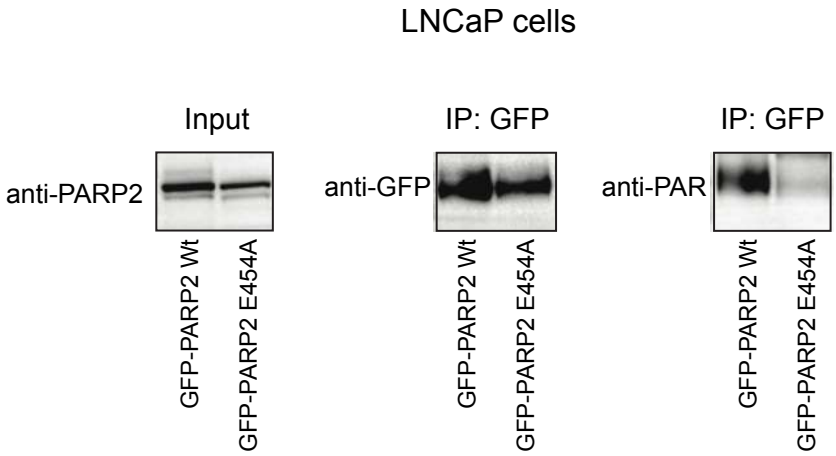

Fig. S9. Analysis of PARP-2 automodification using GFP-PARP-2 wild-type (Wt) and E545A mutant plasmids demonstartes the E454A mutant PARP-2 is enzymatically inactive. Briefly, LNCaP cells (2 x 10e6) were transfected with 10 ug pEGFP-PARP2-WT or E545A mutant plasmid using X-tremeGENE HP DNA Transfection Reagent (Roche) according to the manufacturer's instruction. Cells were collected in RIPA buffer (10 mM Tris/Cl pH 7.5; 150 mM NaCl; 0.5 mM EDTA; 0.1% SDS; 1% TRITON X-100; 1% Deoxycholate) supplied with 1x protein Inhibitor cocktail (Sigma) 24 hours after transfection. The cell lysate was incubated with GFP-Trap magnetic beads (Chromotec) for 2 hours at 4°C. Precipitated products were then washed with washing buffer (10 mM Tris/Cl pH 7.5; 150 mM NaCl; 0.5 mM EDTA) and eluted with 2 x SDS protein loading buffer for western blotting using antibodies against GFP (anti-GFP) and Poly-ADP-ribose (anti-PAR).

SI Appendix, Fig. S10

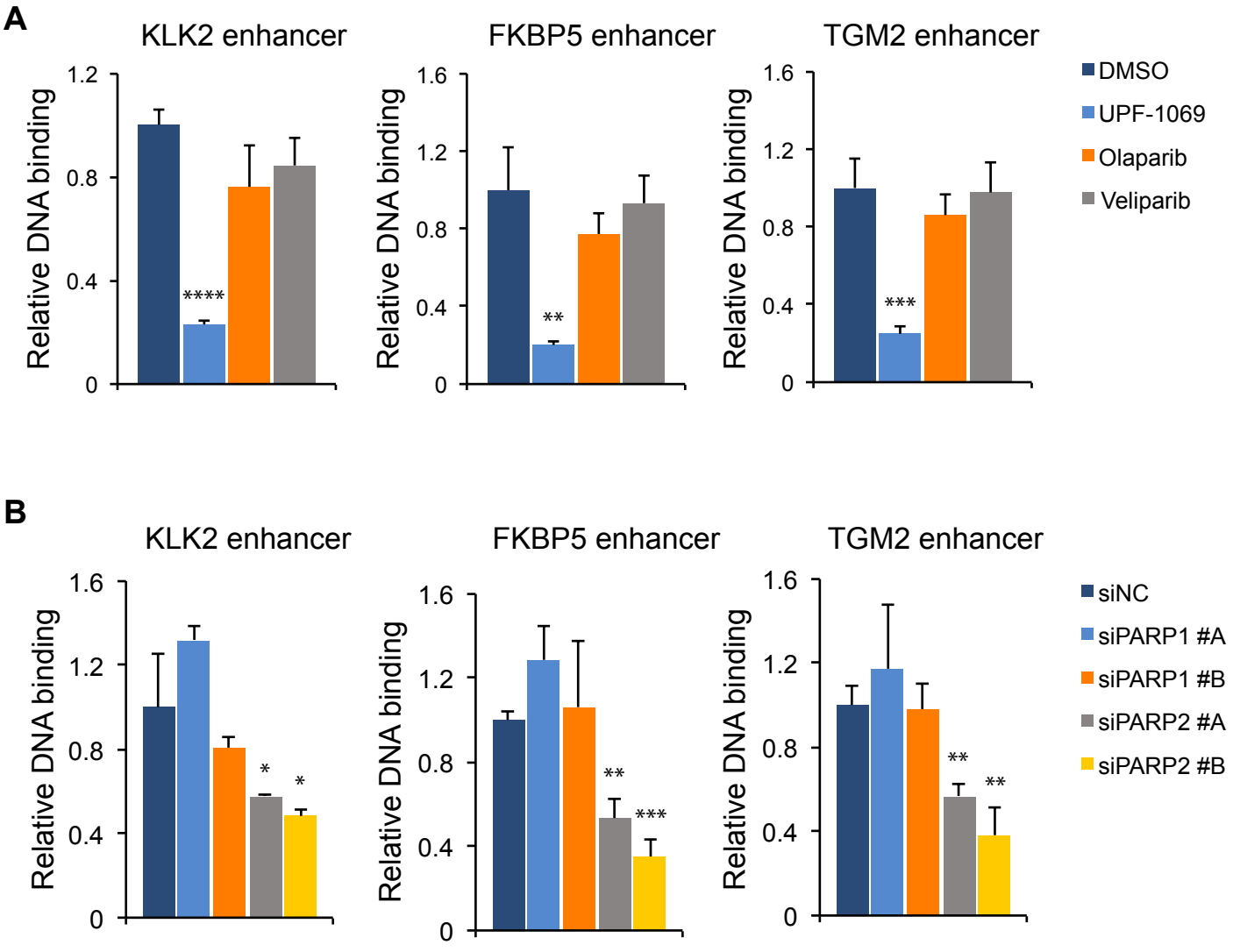

Fig. S10. AR binding at the enhancer regions after PARP-2 inhibition. Relative AR binding was determined by ChIP-qPCR (using TaqMan or SYBR Green method) at the KLK2, FKBP5, and TGM2 loci in LNCaP cells after the treatment with PARP inhibitors (10μM) for 24h **(A)** or 2 days after siRNA knockdown **(B)**. All data represent the mean ± SD from three PCR replicates. Statistical significance was determined by a two-tailed Student's *t*-test. *, $p < 0.05$; **, $p < 0.01$; ***, $p<0.001$.

Primer and probe sequences:
KLK2 enhancer:
Forward, 5'-GGAGAGACAAATGGCGAAAGG-3';
Reverse, 5'-AGGGAACAAGGCTGAGTTGAAC-3';
Prober, 5'-AGCTGAACCTTCTTGGCTCTAGCTGGATCC-3'
FKBP5 enhancer:
Forward, 5'-CCCCCTATTTTAATCGGAGTAC-3';
Reverse, 5'-TTTTGAAGAGCACAGAACACCCT-3'
TGM2 enhancer:
Forward, 5'-GAAGGACCCTGGCCAATTG-3';
Reverse, 5'-TGTTCCCCATCATCCATTCC-3'
Prober, 5'-ATTTTGAGGCCTGGCCACCCTCCT-3'

SI Appendix, Fig. S11

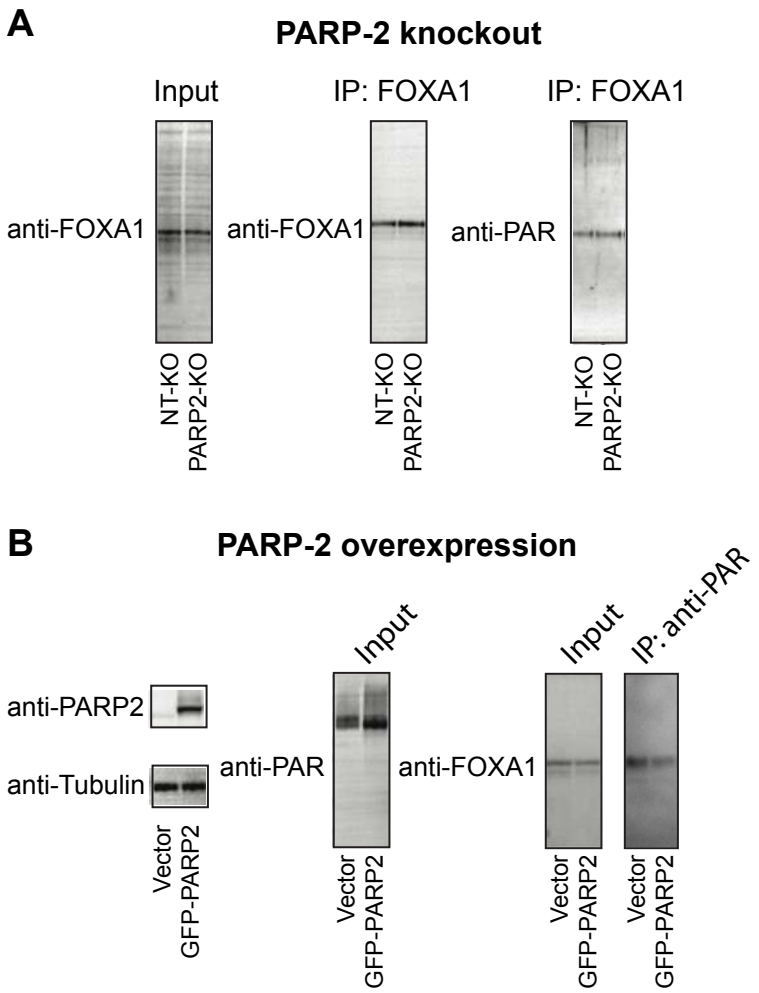

Fig. S11. PARP-2 does not enzymatically modify FOXA1. **(A)** A LNCaP PARP-2 knockout cell line (PARP2-KO) and a non-target control line (NT-KO) were generated through a ribonucleoprotein (RNP) delivery approach (see **Figure 5E**). Immunoprecipitation was performed using antibody against FOXA1. Precipitated products were then washed and eluted with 2 x SDS protein loading buffer for western blotting using antibodies against FOXA1 (anti-FOXA1) and Poly-ADP-ribose (anti-PAR). As shown in the Western blot (right), KO of PARP-2 does not change PARylation of FOXA1. **(B)** LNCaP cells were transfected with GFP-PARP-2 or vector control plasmid using X-tremeGENE HP DNA Transfection Reagent (Roche) according to the manufacturer's instruction. Overexpression of PARP-2 is confirmed by the Western blot using PARP-2 antibody (anti-PARP2) (left). As shown in the Western blot (middle) using anti-PAR, the level of total PARylation is moderately increased in PARP-2 overexpressing LNCaP cells. Immunoprecipitation was performed using anti-PAR. Precipitated products were then washed and eluted with 2 x SDS protein loading buffer for western blotting using anti-FOXA1 (right). Overexpression of PARP-2 does not increase PARylation of FOXA1.

SI Appendix, Fig. S12

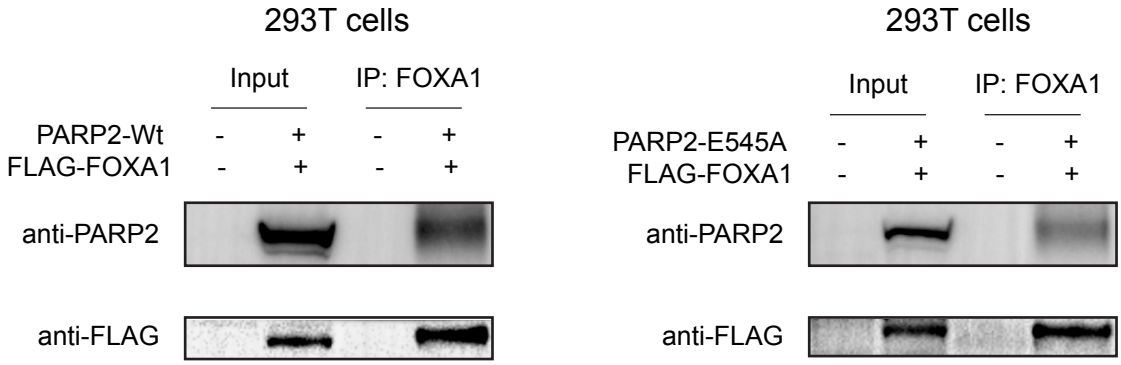

Fig. S12. Both wild-type (Wt) and E545A mutant PARP-2 interact with FOXA1. In a co-immunoprecipitation experiment, 293T cells (2 x 10e6) were co-transfected with 5 ug pEGFP-PARP2-Wt or E545A mutant and 5 ug pCDNA3.1-Flag-FOXA1 plasmids in a 100-mm dish using X-tremeGENE HP DNA Transfection Reagent (Roche). Cells were collected in RIPA buffer (10 mM Tris/Cl pH 7.5; 150 mM NaCl; 0.5 mM EDTA; 0.1% SDS; 1% TRITON X-100; 1% Deoxycholate) supplied with 1x protein Inhibitor cocktail (Sigma) 24 hours after transfection. The cell lysate was precipitated with antibody against FOXA1 (anti-FOXA1) and Protein A/G magnetic beads. Precipitated products were then washed with washing buffer (10 mM Tris/Cl pH 7.5; 150 mM NaCl; 0.5 mM EDTA) and eluted with a 2 x SDS protein loading buffer for western blotting using anti-PARP-2 or anti-FLAG.

SI Appendix, Fig. 13

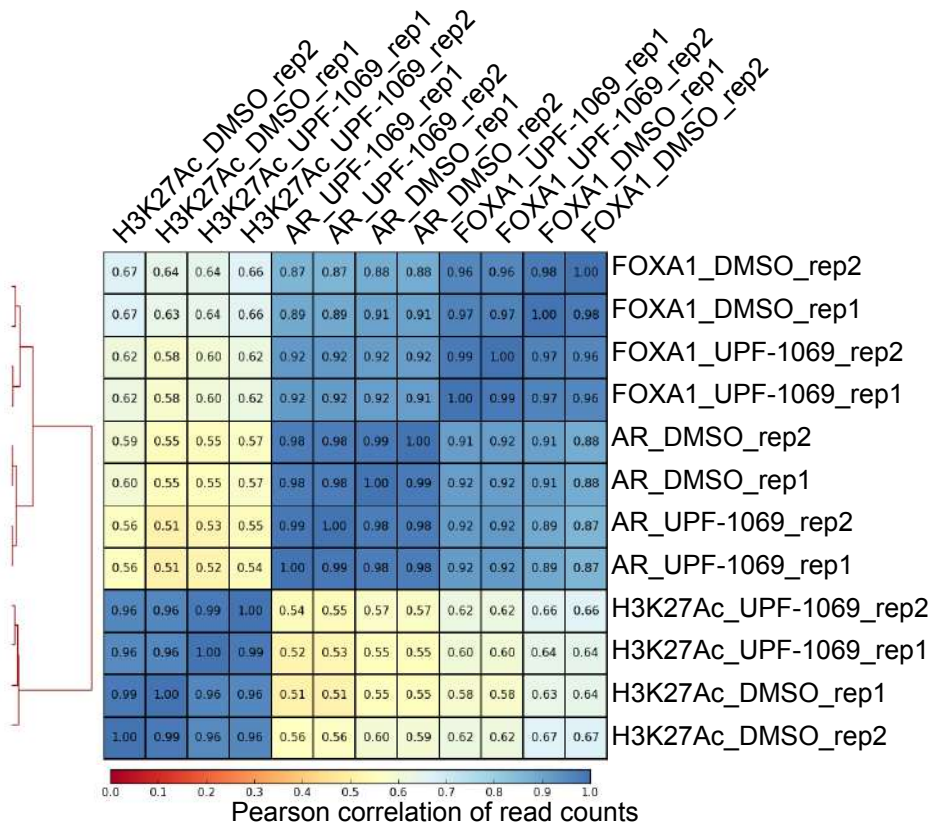

Fig. S13. The reproducibility of ChIP-seq experiments was assessed by calculating the Pearson correlation score and performing an unsupervised hierarchical clustering analysis. Two biological replicates (rep) were used in ChIP-seq.

SI Appendix, Table S1

Small molecule inhibitors		
Name	**Company**	**Cat #**
UPF-1069	Santa Cruz Technology	sc-361396
olaparib	Selleck Chemicals	S1060
veliparib	Selleck Chemicals	S1004
enzalutamide	Selleck Chemicals	S1250
niraparib	MedChemExpress	HY-10619B
rucaparib	MedChemExpress	HY-10617
talazoparib	MedChemExpress	HY-16106
aminobenzamide-3	Trevigen	#4667-50-03
JQ1	a gift from Dr. James E. Bradner's laboratory at DFCI	
PARG inhibitor, Tannic acid	Sigma-Aldrich	#403040
protease inhibitor	Sigma-Aldrich	#4693132001
phosphatase inhibitor	Bimake	B15001

Antibodies		
Name	**Company**	**Cat #**
α-PARP1	Santa Cruz Technology	sc-7150
α-β-Tubulin	Santa Cruz Technology	sc-80011
α-PSA	Santa Cruz Technology	sc-7316
α-HOXB13	Santa Cruz Technology	sc-28333
normal mouse IgG	Santa Cruz Technology	sc-2025
normal rabbit IgG	Santa Cruz Technology	sc-2027
α-PARP2 (IHC)	Active Motif	#39743
α-PARP2 (Western)	Sigma-Aldrich	HPA052003
α-poly(ADP-ribose)	Enzo Life Sciences	ALX804220R100
α-AR	Abcam	ab74272
α-FOXA1	Abcam	ab23738
α-H3K27Ac	Abcam	ab4729
α-GFP	GeneTex	GTX113617
α-flag	Sigma-Aldrich	F1804

siRNA sequences		
Name	Company	Sequence (5' - 3')
siNC	Sigma-Aldrich	MISSION siRNA Universal Negative Control #2 (#SIC002)
siNC1	Sigma-Aldrich	MISSION siRNA Universal Negative Control #1 (#SIC001)
siPARP1 #A	Sigma-Aldrich	CCAUUGAGCACUUCAUGAA
siPARP1 #B	Sigma-Aldrich	GAUUUCAUCUGGUGUGAUA
siPARP2 #A	Sigma-Aldrich	GAAGAAAUUCCUUGACAAA
siPARP2 #B	Sigma-Aldrich	AAGUACUAUCUGAUUCAGCUA

guide RNA sequences		
Name	Company	Sequence (5' - 3')
sgPARP1-A	Sigma-Aldrich	5'-GAGTCGAGTACGCCAAGAGC-3'
sgPARP1-B	Sigma-Aldrich	5'-CGAGTCGAGTACGCCAAGAG-3'
sgPARP2-A	Sigma-Aldrich	5'-CGGCGACGGAGCACCGGCGG-3'
sgPARP2-B	Sigma-Aldrich	5'-CGGCGGCGACGGAGCACCGG-3'

RT-qPCR primers sequences		
Name	Company	Sequence (5' - 3')
KLK2-Forward	Sigma-Aldrich	GCTGCCCATTGCCTAAAGAAG
KLK2-Reverse	Sigma-Aldrich	TGGGAAGCTGTGGCTGACA
KLK3-Forward	Sigma-Aldrich	GGCAGCATTGAACCAGAGGAG
KLK3-Reverse	Sigma-Aldrich	GCATGAACTTGGTCACCTTCTG
TMPRSS2-Forward	Sigma-Aldrich	CCTGCAAGGACATGGGTATA
TMPRSS2-Reverse	Sigma-Aldrich	CCGGCACTTGTGTTCAGTTTC
FKBP5-Forward	Sigma-Aldrich	TGGGGCTTTCTTCATTGTTC
FKBP5-Reverse	Sigma-Aldrich	GCGGAGAGTGACGGAGTC
NKX3.1-Forward	Sigma-Aldrich	CAGATAAGACCCCAAGTGCC
NKX3.1-Reverse	Sigma-Aldrich	CAGAGCCAGAGCCAGAG
AR-Forward	Sigma-Aldrich	AAGCTTCTGGGTGTCACTATGGA
AR-Reverse	Sigma-Aldrich	GTTTCCCTTCAGCGGCTCTT
PARP1-Forward	Sigma-Aldrich	TCTGCCTTGCTACCAATTCC
PARP1-Reverse	Sigma-Aldrich	GATGGGTTCTCTGAGCTTCG
PARP2-Forward	Sigma-Aldrich	TGTTGTTGTTGAACTGGAGATTG
PARP2-Reverse	Sigma-Aldrich	TGTTGTTGTTGAACTGGAGATTG
GAPDH-Forward	Sigma-Aldrich	GTCATGGGTGTGAACCATGAGA
GAPDH-Reverse	Sigma-Aldrich	GGTCATGAGTCCTTCCACGATAC

ChIP-qPCR primer and prober sequences		
Name	Company	Sequence (5'-3')
PSA enhancer-Forward	Sigma-Aldrich	GCCTGGATCTGAGAGAGATATCATC
PSA enhancer-Reverse	Sigma-Aldrich	ACACCTTTTTTTTTCTGGATTGTTG
PSA enhancer-probe	Sigma-Aldrich	TGCAAGGATGCCTGCTTTACAAACATCC
Control region-Forward	Sigma-Aldrich	TCCTGCCCTGGAGAACTTAAAG
Control region-Reverse	Sigma-Aldrich	TAGTGGTCAGCAGGCAGTGC
Control region-probe	Sigma-Aldrich	CTGCACTGGGTGCCTACTGCCTTGTAA